AN INVESTIGATION OF THE USE OF SPIN-STABILIZED CUBES AS FRAGMENT SIMULATORS IN ARMOR EVALUATION

Randall L. Schamberger

Air Force Institute of Technology
Wright-Patterson Air Force Base, Ohio

June 1971

Unclassified
Security Classification

AD-769801

DOCUMENT CONTROL DATA - R & D

(Security classification of title, body of abstract and indexing annotation must be entered when the overall report is classified)

1. ORIGINATING ACTIVITY (Corporate author) Air Force Institute of Technology (AFIT-EN) Wright-Patterson AFB, Ohio 45433	2a. REPORT SECURITY CLASSIFICATION Unclassified 2b. GROUP

3. REPORT TITLE

AN INVESTIGATION OF THE USE OF SPIN-STABILIZED CUBES AS FRAGMENT SIMULATORS IN ARMOR EVALUATION

4. DESCRIPTIVE NOTES (Type of report and inclusive dates)

AFIT Thesis

5. AUTHOR(S) (First name, middle initial, last name)

Randall L. Schamberger
Captain USAF

6. REPORT DATE June 1971	7a. TOTAL NO. OF PAGES ~~90~~ 104	7b. NO. OF REFS 30
8a. CONTRACT OR GRANT NO. N/A b. PROJECT NO. 7360 c. Task N. 736006 d.	9a. ORIGINATOR'S REPORT NUMBER(S) AFIT Thesis GAM/MC/71-8 9b. OTHER REPORT NO(S) (Any other numbers that may be assigned this report) N/A	

10. DISTRIBUTION STATEMENT

Approved for public release; distribution unlimited.

11. SUPPLEMENTARY NOTES Approved for public release; IAW AFR 190-17 JERRY C. HIX, Captain, USAF Director of Information	12. SPONSORING MILITARY ACTIVITY Air Force Materials Laboratory Wright-Patterson AFB, Ohio 45433

13. ABSTRACT

An investigation was made of the use of cubes as fragment-simulators for armor evaluation and testing. One-quarter inch steel cubes were launched from a rifled barrel in an attempt to induce stability through spin stabilization. Specially molded lexan sabots were used to launch the cubes in the three predominant orientations: flat, edge, and point. The success rate of impact orientation predictability was high enough to warrant further consideration of cubes as fragment simulators.

V_{50} ballistic limits were determined for four armor materials under flat, edge, and point impacts. The ballistic limits determined with cubes differed considerably from those determined with standard fragment-simulating projectiles of the same mass. Metallic armor materials failed at higher velocities for the cubes, while fibrous armor materials were penetrated at lower velocities by the cubes. An alternate method for determining ballistic limits with cubes is also presented.

Drag coefficients were determined for the three predominant orientations over the range of Mach numbers 0.5 to 3.5 and found to be generally higher than those previously measured by investigators who assumed cubes tumbled in flight.

DD FORM 1 NOV 1473

Unclassified
Security Classification

AN INVESTIGATION OF THE USE OF SPIN-STABILIZED CUBES AS FRAGMENT-SIMULATORS IN ARMOR EVALUATION

THESIS

GAM/MC/71-8

Randall L. Schamberger
Captain USAF

AN INVESTIGATION OF THE USE OF SPIN-STABILIZED CUBES AS FRAGMENT-SIMULATORS IN ARMOR EVALUATION

THESIS

Presented to the Faculty of the School of Engineering

of the Air Force Institute of Technology

Air University

in Partial Fulfillment of the

Requirements for the Degree of

Master of Science

by

Randall L. Schamberger, B.S., A.A.
Captain USAF

Graduate Aerospace-Mechanical Engineering

June 1971

Preface

This thesis was initiated as a result of a special study by the Joint Interservice Body Armor Committee on the use of cubes and spheres as fragment simulators.

I wish to thank Mr. Hallock F. Swift of the University of Dayton Research Institute for his initial suggestions in undertaking this study; Mr. Gordon H. Griffith of the Air Force Materials Laboratory for the use of range facilities; Mr. Robert S. Bertke of the Conventional Projectiles Facility for his enthusiastic assistance; and my faculty thesis advisor, Major William Goldberg, for his patience and guidance.

A special thanks goes to Mr. Michael F. Lehman, Mr. James E. Green, and Mr. Charles E. Acton for their outstanding technical support and untiring efforts toward the completion of this study, and to Captain Thomas C. Finley for the development of the computer program used in computing impact angles.

Randall L. Schamberger

Contents

Contents (cont'd)

List of Symbols

Symbol	
A	Area or projected area
B	Axial moment of inertia
C	Transverse moment of inertia
C_D	Drag coefficient
D	Drag force
E	Prefix for edge-launched cube shot number
F	Prefix for flat-launched cube shot number
L	Suffix for cube shot number fired on long range
M	Mach number
N	Overturning moment
P	Prefix for point-launched cube shot number
S	Suffix for cube shot number fired on short range
V_1	Average velocity between velocity screens #1 and #2
V_2	Average velocity between velocity screens #2 and #3
V_{50}	Velocity at which there is 50% probability of complete target penetration
a	Distance from mass center of cube to center of pressure
d	Longest edge of yaw card silhouette (hexagon)
e	Intermediate edge of yaw card silhouette (hexagon)
f	Shortest edge of yaw card silhouette (hexagon)
g	Acceleration of gravity
$\bar{i}\,\bar{j}\,\bar{k}$	Unit vectors

Symbol	
k	Length of cube face diagonal
l	Length of cube edge
m	Mass
$\bar{n}$	Unit vector normal to impact plane
n	Length of cube face diagonal projection on yaw card
s	Stability factor
t	Time
x	Range position on flight trajectory
γ	Error angle between unit normal $\bar{n}$ and perfect impact orientation vectors
δ	Angle of projectile yaw (angle between longitudinal axis of projectile and trajectory of projectile center of gravity)
ϵ	Largest impact angle
θ	Smallest impact angle
μ	Coefficient of overturning moment
ρ	Density
ϕ	Intermediate impact angle
ω	Rate of spin

List of Figures

List of Figures (cont'd)

List of Tables

List of Tables (cont'd)

Abstract

An investigation was made of the use of cubes as fragment-simulators for armor evaluation and testing. One-quarter inch steel cubes were launched from a rifled barrel in an attempt to induce stability through spin stabilization. Specially molded lexan sabots were used to launch the cubes in the three predominant orientations: flat, edge, and point. The success rate of impact orientation predictability was high enough to warrant further consideration of cubes as fragment simulators.

V_{50} ballistic limits were determined for four armor materials under flat, edge, and point impacts. The ballistic limits determined with cubes differed considerably from those determined with standard fragment-simulating projectiles of the same mass. Metallic armor materials failed at higher velocities for the cubes, while fibrous armor materials were penetrated at lower velocities by the cubes. An alternate method for determining ballistic limits with cubes is also presented.

Drag coefficients were determined for the three predominant orientations over the range of Mach numbers 0.5 to 3.5 and found to be generally higher than those previously measured by investigators who assumed cubes tumbled in flight.

AN INVESTIGATION OF THE USE OF SPIN-STABILIZED CUBES AS FRAGMENT-SIMULATORS IN ARMOR EVALUATION

I. Introduction

The use of fragment-producing high explosive warheads against material and personnel in limited warfare has led to extensive investigation of fragments and their effect on armor materials. The evaluation of armor materials involves the determination of the depth of projectile penetration, ballistic limit, and residual velocities of fragments after armor penetration.

Background

In the 1940's, the Watertown Arsenal developed a fragment-simulator that has since become a standard for armor testing (Ref 23:3). Fig. 1 illustrates the standard fragment-simulating projectile shape. The geometric similarity to actual projectiles makes them

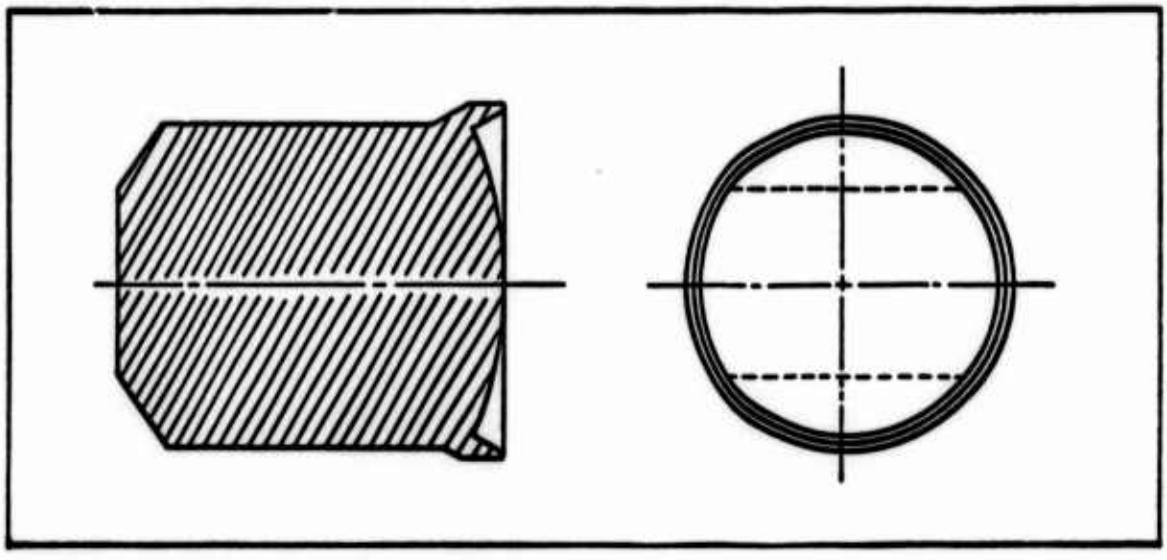

Fig. 1. Fragment-Simulating Projectile Used in the Evaluation of Personnel Armor (From Ref 23:10)

easily adaptable for launching in conventional gun barrels. All standard calibers from .15 to .50 and 20 mm are currently available. Most armor evaluation tests are presently being conducted with this fragment-simulator geometry.

Muldoon (Ref 23) originally determined the drag coefficients for the simulators and found good agreement with earlier drag studies conducted with actual bomb fragments (Ref 25). Later, Heppner and Steedman, with more sophisticated measuring equipment, conducted similar drag studies and compared drag coefficients obtained with those determined by Muldoon and found the results to be consistent except in the velocity region below 1500 ft/sec, where Muldoon's values of C_D were slightly higher (Ref 10:10).

The penetration characteristics of standard projectiles are dependent on the nose shape and velocity of the projectile. Warnis (Ref 28) fired actual bomb fragments (15 grain) against Nu-wood wallboard and found that the presented area at impact had no effect on penetration depth at velocities above 3000 ft/sec. However, at velocities below 1000 ft/sec the presented area did have an effect on the penetration depth.

Fragments can assume many shapes, but Warnis classified the fragments according to the ratios of length, width, and depth of the fragment. The general shapes of all of his fragments, however, were rectangular parallelepipeds (Ref 28:5).

Ipson (Ref 13) conducted impact and in-flight orientation studies using parallelepipeds and found that the projectiles tended to strike the targets with the large face first, irrespective of the orientation in which they were launched. Yaw cards were placed along the trajectory to record the gyrations of the projectiles in flight. A system of measuring the angles and sides of the yaw card perforations was devised to record the orientation of the projectiles in flight.

The orientation of the projectile was also classified according to its predominant orientation as it penetrated the yaw card: as a flat surface, an edge, or a point. Cubes can also be used to achieve these orientations, but the method of Ipson cannot be used to study the actual motion of the cubes. The tri-dimensional symmetry of the cubes prevents the establi nt of any type of reference system using yaw cards for studying their in-flight motion. Cubes, however, have been studied extensively for use as fragment-simulators.

Hansche and Rhinehart (Ref 9) determined the air drag on one-quarter and three-eighths inch cubes at Mach numbers 0.5 to 3.5 and the shape of the drag curves compared very favorably with earlier drag studies on spheres by Charters and Thomas (Ref 2). Clark and Harris (Ref 3), May and Witt (Ref 21), and Hodges (Ref 12) all conducted additional drag studies on spheres that further substantiated the earlier results of Charters and Thomas.

Hansche and Rhinehart made no attempt to determine specific drag as a function of cube orientation since they assumed that the

cubes tumbled in flight. This assumption was corroborated by examination of the perforations in the velocity screens (Ref 10:84). Instead, they plotted the product C_DA from the drag equation (Eq 11) vs. the Mach number. The values of C_DA versus Mach number are plotted in Fig. 2.

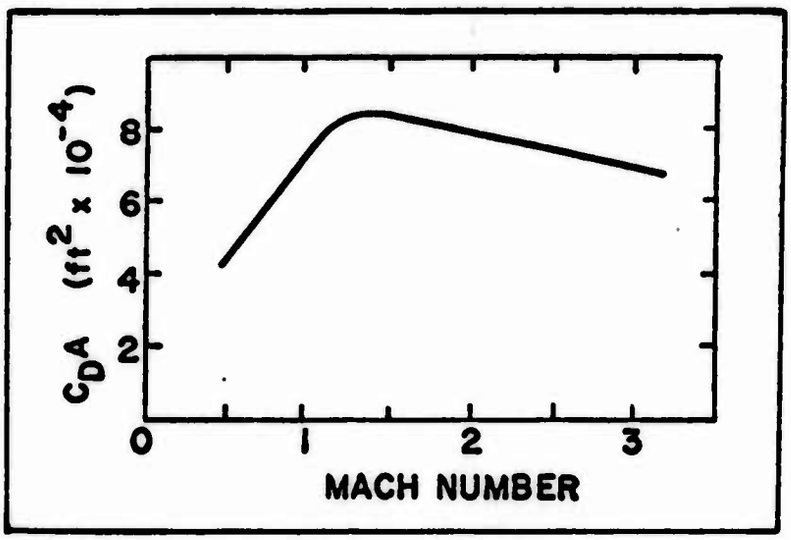

Fig. 2. C_DA vs. Mach Number For 1/4 inch Cubes (From Ref 10:84)

Dunn and Porter (Ref 6:13) and Jones (Ref 15:722), in other cube drag studies, also assumed random orientation of the cubes in flight.

Van Caneghem and Pless, in summarizing the results of a round-robin armor material evaluation by eight Department of Defense weapons ranges, noted that cubes were not randomly oriented at impact (Ref 27:22). The primary purpose of this testing program was to establish ballistic limit standardization procedures with spheres and cubes. Only two of the eight ranges kept records of impact

orientation, but these ranges showed a much higher incidence of flat impacts. Therefore, the study concluded that random impacts (equal probability of the three predominant orientations (flat, edge, and point) were not achievable and recommended that cubes not be used for fragment studies (Ref 27:5). It was also noted that ballistic limit values varied widely among the ranges for cube impacts, whereas, ballistic limits were in close agreement with sphere impacts. This result demonstrated the influence of cube orientation on ballistic penetration (Ref 27:5).

It should be noted that all cube studies mentioned previously employed only smoothbore barrels. No attempt was made to stabilize the cubes or predict their orientation. Hansche and Rhinehart launched their cubes from .30 and .50 caliber smoothbore barrels by stuffing wads of cloth behind the cubes to act as pushers (Ref 9:83). Dunn and Porter used a similar method to launch the cubes (Ref 6:13).

Ewing designed a square-bore cube launcher, but his intention was to devise a means of avoiding sabot contamination of targets placed close to the gun muzzle (Ref 7:5). Whiteford and Reagan used this gun to study the penetration characteristics of three sizes of cubes fired into wallboard, but no correlation to cube impact orientation was made (Ref 29:9).

Purpose

All of the cube studies performed to date have accepted the inevitability of a tumbling cube and the inability of the testing agency

to accurately predict the orientation of the cube at impact. If it were possible to accurately predict the orientation of the cube at impact, a wealth of knowledge could be gained about the characteristics of various armor materials under fragment impact.

The purpose of this study is to develop a method of predetermining impact orientation of cubes for materials testing and to examine several armor materials for ballistic limits under the three predominant impact orientations. In conjunction with this testing, drag coefficients for the three orientations will be determined.

II. Theory

Spin-Stabilization of the Cubes

It is an established fact among ballisticians that a projectile fired from a gun maintains its stability because of the spin imparted to it by the rifling in the barrel. Without this spin-stabilization, the projectile tumbles in flight and tends to assume an orientation of maximum drag (Ref 5:65).

When spin is imparted to a projectile, other forces and moments are added to the original lift and drag forces. References 17, 18, 19, and 30 thoroughly examine the forces acting on a spinning projectile. These forces and moments, in practice, are determined experimentally and suitable force and moment coefficients are introduced into the stability equations.

A simplified approach to the stability problem states that, for stability of a spinning projectile, the stability factor, s, must be equal to or greater than one. The stability factor is defined as

$$s = \frac{B^2 \omega^2}{4 C \mu} \geq 1 \qquad \text{(Ref 30:27)} \qquad (1)$$

where B is the axial moment of inertia of the body

ω is the projectile spin in rad/sec

C is the transverse moment of inertia of the body

μ is the coefficient of overturning moment. This is a proportionality factor between the overturning moment, N, and the angle of yaw, δ, where $N = \mu \sin \delta$.

Wind tunnel tests or a series of yaw cards can be used to determine the coefficient, μ, for standard projectiles, however, there is no way to determine the exact motion of a cube as it moves along its trajectory. The tri-dimensional symmetry of the cube prevents any study of its motion in flight using yaw cards.

The simplified theory of a sleeping top is often used to determine minimum spin for the stability of a projectile in flight. This stability equation states, that for a spinning top to be stable,

$$\omega^2 \geq \frac{4Cmga}{B^2} \qquad \text{(Ref 26:440)} \qquad (2)$$

where ω is the minimum spin rate in rad/sec

C is the transverse moment of inertia of the body

mg is the weight of the top acting through the mass center

a is the distance from the mass center to point of contact with the surface

B is the axial moment of inertia of the body.

This equation may be adapted to a spinning projectile by substituting the drag force, D, on a projectile for the weight term, mg, and letting a be the distance from the mass center to the center of pressure on the projectile. The equation thus becomes

$$\omega^2 \geq \frac{4CDa}{B^2} \qquad \text{(Ref 26:441)} \qquad (3)$$

Eq (3) was used to determine the barrel twist required to stabilize the cubes in flight so that launch and impact orientations

would be identical. Appendix C details the calculations for determining the twist required for each of the predominant orientations. Using the standard one-quarter inch cube dimensions and mass, the required twists were computed to be one turn in 37 inches for flat impact, one turn in 31 inches for edge impact, and one turn in 28 inches for point impact. A barrel with one turn in 28 inches was chosen for the test firings.

Determination of Cube Impact Orientation

The orientation of the cube at impact can be determined by placing a yaw card immediately in front of the target. Measurement of the perforation silhouette reveals the impact orientation of the cube. Fig. 3 illustrates silhouettes of the three perfect orientation positions: flat, edge, and point. The exact orientation of any cube impact can be determined by applying a trigonometric solution.

Impact orientation is expressed as a function of three angles formed by the three orthogonal edges of the cube with the yaw card

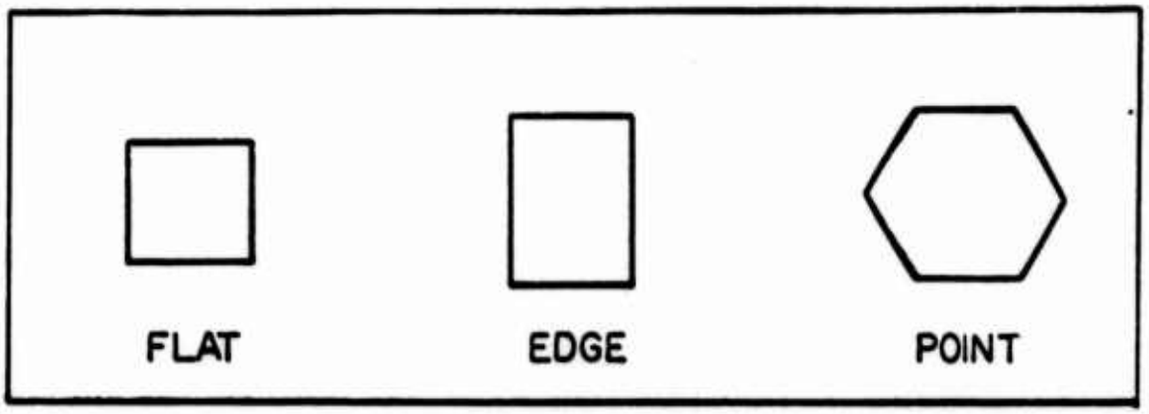

Fig. 3. Yaw Card Impact Silhouettes

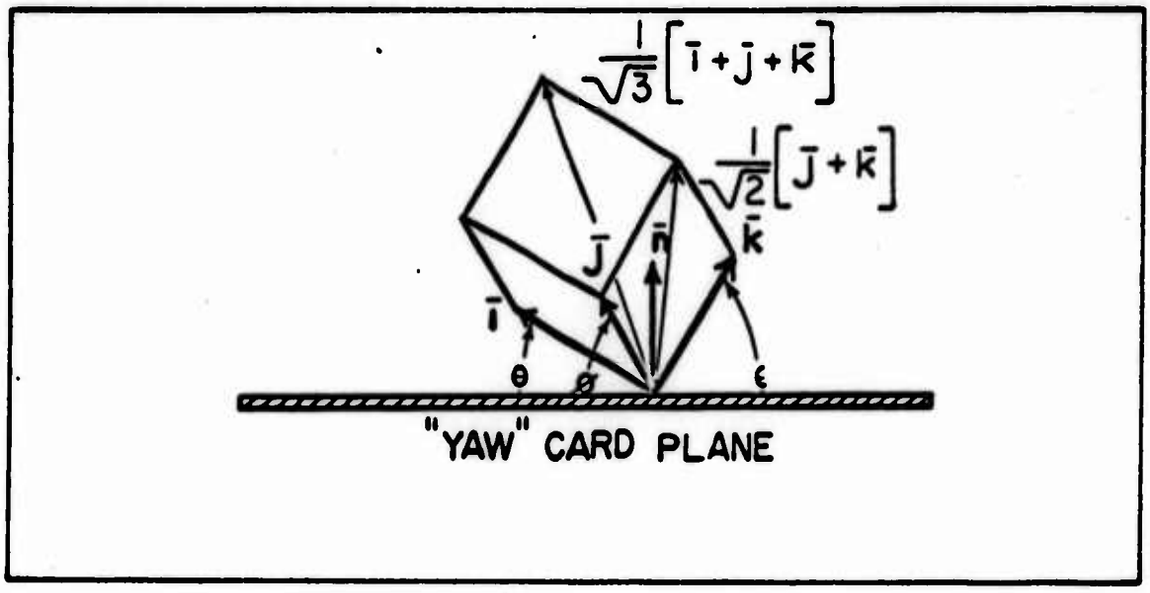

Fig. 4. Cube Impact Orientation Angles

plane. Fig. 4 illustrates these angles. By convention, the angle θ will always be the smallest angle; the angle ϕ, the intermediate angle; and the angle ϵ, the largest angle.

The cubes do not hit perfectly flat, on the edge or on the point every time, so predominant orientations are recorded. From Fig. 4 and analytic geometry it is seen that

$$\cos^2(90°-\theta) + \cos^2(90°-\phi) + \cos^2(90°-\epsilon) = 1$$

$$\text{or} \qquad \sin^2\theta + \sin^2\phi + \sin^2\epsilon = 1 \tag{4}$$

A Gaertner micro-slide comparator was used to measure the edges of the impact silhouettes and the lengths of the parallel edges were averaged. A perfectly flat impact yields a square silhouette. Fig. 5 illustrates the method for determining the impact angles for the edge and point impacts.

For the edge impact $\theta = 0^c$ (5)

and $\cos[45^\circ - \phi] = \frac{n}{k}$

or $\phi = 45^\circ - \cos^{-1}\left(\frac{n}{k}\right)$ (6)

and $\epsilon = 90^\circ - \phi$ (7)

For the point impact $\cos\theta = \frac{d}{\ell}$ (8)

where d is the longest edge of the impact silhouette and ℓ is the cube edge length,

$$\cos\phi = \frac{e}{\ell} \tag{9}$$

where e is the intermediate edge of the impact silhouette,

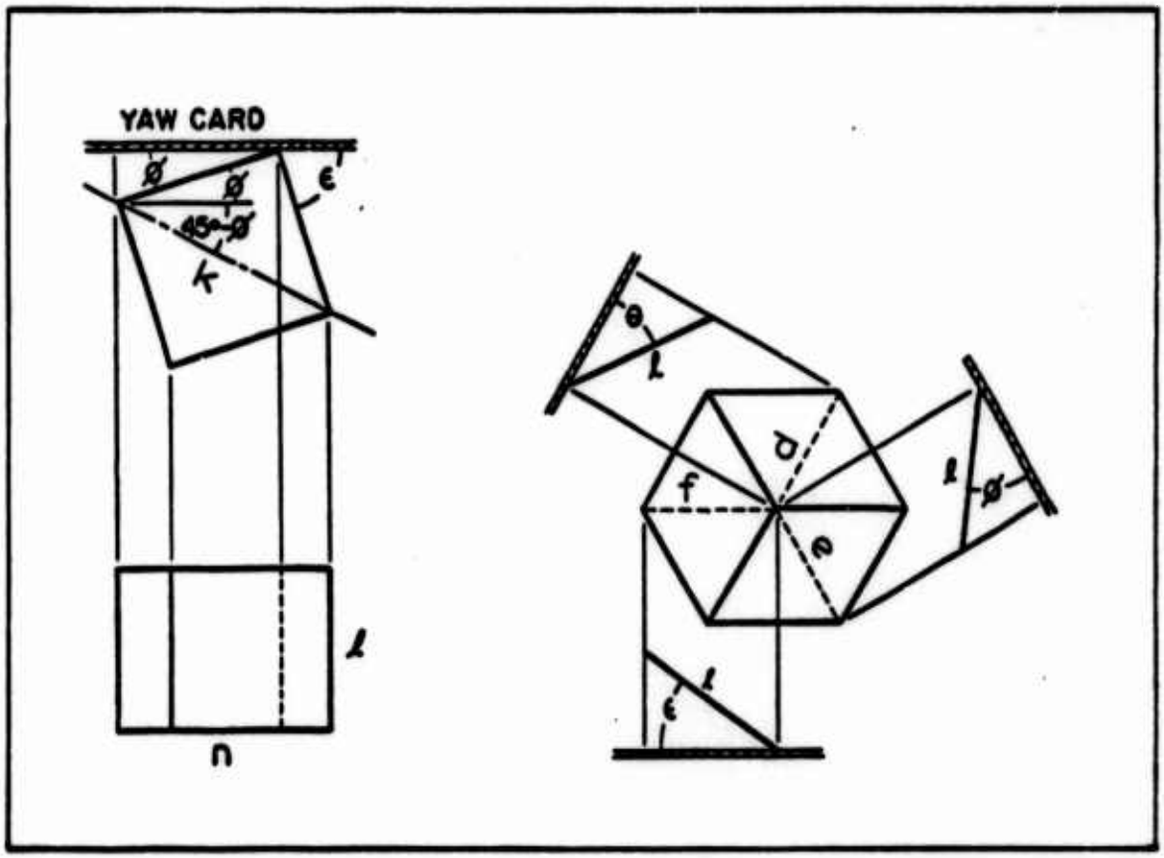

Fig. 5. Determination of Impact Angles for Edge and Point Impacts

$$\text{and } \cos \epsilon = \frac{f}{\ell} \qquad (10)$$

where f is the shortest edge of the impact silhouette.

The calculated impact angles are substituted into equation (4). The errors in measurement of silhouette edges will cause the summation to be equal to some number greater or less than one. The equation must be normalized to force the function value to one. This causes the angles θ, ϕ, and ϵ to change. The angle θ is assumed to have the least percentage of measured error and the angle ϵ, the greatest percentage of measured error. The normalizing procedure does not affect this characteristic.

The adjusted angles are now used to determine the predominant impact orientation. The predominant impact orientation is determined by examining the error angles relative to unit normal, $\bar{n}$, to the yaw card plane. In Fig. 4 the unit vectors $\bar{i}$, $\bar{j}$, and $\bar{k}$ are coincident with the edges of the cube. The direction of the unit normal, $\bar{n}$, is seen to be $\sin\theta\,\bar{i} + \sin\phi\,\bar{j} + \sin\epsilon\,\bar{k}$.

For perfect flat impacts, the unit vector $\bar{k}$ will coincide with the unit normal $\bar{n}$. The vector $\frac{1}{\sqrt{2}}\bar{j} + \frac{1}{\sqrt{2}}\bar{k}$ will coincide with the unit normal for perfect edge impacts and the vector $\frac{1}{\sqrt{3}}\bar{i} + \frac{1}{\sqrt{3}}\bar{j} + \frac{1}{\sqrt{3}}\bar{k}$ will coincide with the unit normal for point impacts. Thus, the angles between each of these vectors and the unit normal can be determined by taking the dot product of each of these vectors with the unit normal. These angles represent the error angles for each of the three impact orientations. The smallest error angle indicates the predominant

orientation. When all three error angles are equal, there is no predominant orientation. This occurs when $\theta = 16.4^{\circ}$, $\phi = 21.5^{\circ}$, and $\epsilon = 62.4^{\circ}$.

It is assumed that the yaw cards have negligible influence on the orientation of the cube during penetration. Karpov notes that photographic print paper yaw cards have negligible effects on small conventional projectiles (Ref 16:14). Greenwood and Maroney conducted tests for the effect of yaw cards on stability factors, but most of their work was done on large projectiles with relatively heavy yaw cards placed in series of ten cards and more (Ref 8:5).

Determination of Drag Coefficients and Impact Velocities

The equation of motion for a projectile in air can be written in the form

$$D = -m\frac{dv}{dt} = C_D \frac{\rho A V^2}{2} \tag{11}$$

where D is the drag force

m is the mass of the projectile

$\frac{dv}{dt}$ is the acceleration

ρ is the air density

A is the presented area of the projectile

V is the velocity

C_D is the drag coefficient

This equation may be integrated to give

$$\ln\left(\frac{v}{v_o}\right) = -C_D \frac{\rho A}{2m} \left(x - x_o\right) \tag{12}$$

$$V_{impact} = V_o \exp\left[-C_D \frac{\rho A}{2m} \left(x - x_o\right)\right] \tag{13}$$

where v is the velocity at x and v_o is the velocity at x_o, and C_D is assumed to be constant over the velocity range considered.

Knowing the velocities at any two points, the drag coefficient may be calculated from Eq (12). Using this value of C_D, the impact velocity, V_{impact}, may be calculated from Eq (13) if the distance to the target is known.

Other Considerations

Projectile spin has been neglected in determining the penetration characteristics of the cubes. Krafft used .30 caliber bullets to show that sliding friction of a spinning projectile accounts for only 3% of the energy loss of an impacting projectile. At ballistic velocities, the event is of such short duration that friction heat cannot be conducted, therefore, the target metal melts and the surface friction is reduced to just maintain the interface at the melting point (Ref 20:1248).

III. Experimental Procedures

One-quarter inch cubes, made from 4150 steel, were launched from a .50 caliber rifled barrel with a one turn in 28 inches twist. The cubes were machined to 0.250 ± .003 inches and the masses of the cubes were 31.0 ± .7 grains. The hardness of the cubes was Rockwell C36 ± 2. One-quarter inch cubes were chosen primarily because they were the largest that would fit the .50 caliber barrel in all three orientations.

Pre-molded lexan sabots were used to hold the cubes in the three preferred launch orientations. A complete description of the sabots is given in Appendix B.

The cubes were hand-fitted into the two piece sabots and the sabots were press-fitted into the .50 caliber barrel. A dual-threaded connector was used to attach a .30 caliber chamber to the .50 caliber barrel (see Fig. 15, Appendix A). A circular disc of five mil (0.005 inch) mylar was coated on each side with vacuum grease and placed between the barrel and the chamber. The disc was used to assure a reproducible build up of gases in the chamber. When the disc ruptured, an even load distribution was imposed on the sabot. 300 H and H magnum cartridges were modified to fit the chamber by removing the neck portion of the casing.

Spin-Stabilization of the Cubes

Preliminary testing to study cube stability was done in the Fragment Simulator Facility (Ref 1:14). Initially, one hundred cubes

were fired through yaw cards to compare the cube orientation in flight with the launch orientation. In addition to the one turn in 28 inches barrel, a one turn in 15 inches, a one turn in 12 inches and a smoothbore barrel were tested. High speed photographs were taken of sabot separation and cube impact. Numerous sabot configurations were also tried at this time.

The overall results of this testing showed that the one turn in 28 and the one turn in 15 inches twist barrels had the highest success rates. The one turn in 12 inches barrel introduced a spiral trajectory in a large number of shots due to overspin. The smoothbore barrel was discarded because of inadequate sabot separation. Some wild shots were fired from the one turn in 15 inches barrel on the long range, again, presumably due to overspin of the projectile. The one in 28 barrel afforded the best control and success rate.

Ballistic Limits of Selected Armor Materials

Ballistic limits were determined for four armor materials: two homogeneous and two non-homogeneous. The materials tested were

2024 T-351 Aluminum plate (0.250 inch, 57.6 oz/ft^2)

1030 Hot-Rolled Steel plate (0.125 inch, 81.7 oz/ft^2)

Ballistic felt (0.50 inch, 6.0 oz/ft^2)

12-Layer Ballistic Nylon (19.0 oz/ft^2).

Initial firings were conducted on a range (Fig. 14) that was 35 feet 7-1/2 inches from gun muzzle to target, with three velocity

screens placed at 12-feet intervals. The distance from the Number 3 screen to the target was 3 feet 3-3/4 inches.

At velocities below 1000 ft/sec, it was discovered that cube trajectories were erratic and as a result, some shots hit the Number 3 velocity screen holder. The range was shortened to 17 feet 3-1/2 inches with the velocity screens placed at five feet intervals and no further problems were encountered. The distance from the Number 3 velocity screen to the target was 9-1/2 inches. Shot numbers in Appendix D are suffixed with an "L" or "S" to indicate Long or Short range firing.

Velocities were determined by measuring the times to traverse the distances between the three velocity screens. Perforation of the Number 1 velocity screen started the timing sequence. Perforation of the Number 2 velocity screen stopped the first timer and started the second timer. Perforation of the Number 3 velocity screen stopped the second timer. The velocity ratio of V_1 and V_2 was used to calculate the drag coefficient and predict the impact velocity. Velocity screen distances were measured before and after each day of firing and no deviations were noted.

If a cube hit the target in an orientation other than its launch orientation (as determined from the yaw card), this data was used for the ballistic limit study under the actual impact orientation. It was assumed that the orientation of the cube did not change appreciably between the last measured velocity position and the target, thus the velocity drop to the target was calculated using the appropriate drag

data for that orientation. Eq (13) was used for all V_{impact} calculations.

V_{50} ballistic limits (as defined by the Ballistic Research Laboratories) were determined for all the materials. The criteria for a V_{50} ballistic limit is that the probability of complete penetration of the target is 50%. The V_{50} value is obtained by taking the five highest partial penetration velocities and the five lowest complete penetration velocities within a 125 ft/sec spread and averaging the ten values (Ref 4:10).

A 0.020 inch 2024-T3 Aluminum witness plate is placed six inches behind the target material to provide the protection criteria. Penetration of the witness plate (such that daylight can be seen) by the projectile or target debris qualifies as a complete penetration. Failure in penetration of the witness plate is a partial penetration (Ref 4:8). In some cases, especially in the lower velocity range, it was not possible to obtain the required ten shots. Such deviations are noted in the Results and Discussion section.

Determination of Drag Coefficients

Eq (12) was used to compute the coefficient of drag, C_D, for the three orientations. Only shots with identical launch and impact orientation were used in determining C_D. The Mach Number was computed using the projectile velocity at the midpoint in the trajectory, that is, the mean value of V_1 and V_2 velocity measurements.

Velocity losses in velocity screen penetration were considered negligible. Hansche and Rhinehart used similar screens and found by ballistic pendulum tests that the velocity loss per screen was approximately three feet per second (Ref 9:83). Several shots in the current study were fired through the three velocity screens with a dummy screen set up between Number 2 and Number 3 velocity screens. Velocity drop was compared for shots fired with and without the dummy screen and the screen loss was found to be approximately six feet per second. These shots were fired in the 1500-1600 ft/sec velocity range. This velocity loss was considered negligible in light of other probable errors in velocity measurements.

It was assumed in the drag calculations that the presented area for each launch orientation remained constant throughout the trajectory. The Results and Discussion section will discuss this assumption more fully.

IV. Results and Discussion

Spin-Stabilization of the Cubes

A total of 273 cubes were fired in this study. The successful launch rates for each of the three orientations were flats, 89%; edges, 58%; and points, 49%. It was originally felt that the stability would be much better at the higher velocities, but examination of Figs. 6, 7, and 8 reveal that no real strength can be given to this assumption. Table I gives the percentage of each type of impact for specific launch orientation.

Table I

Impact Orientations for Specific Launch Orientations

Flat Launch (92)		Edge Launch (95)		Point Launch (86)	
Point	1%	Flat	9%	Flat	14%
Edge	10%	Point	33%	Edge	37%
Flat	89%	Edge	58%	Point	49%

Tables III-V in Appendix D list each shot by launch orientation and give impact angles and predominant impact orientation. The prefixes "F", "E", and "P" designate flat, edge, and point launches, respectively.

The original intent of this study was to maintain a five degree tolerance on the intended perfect impact angles, but it was observed very early in the study, that except for the flat launches, only a small

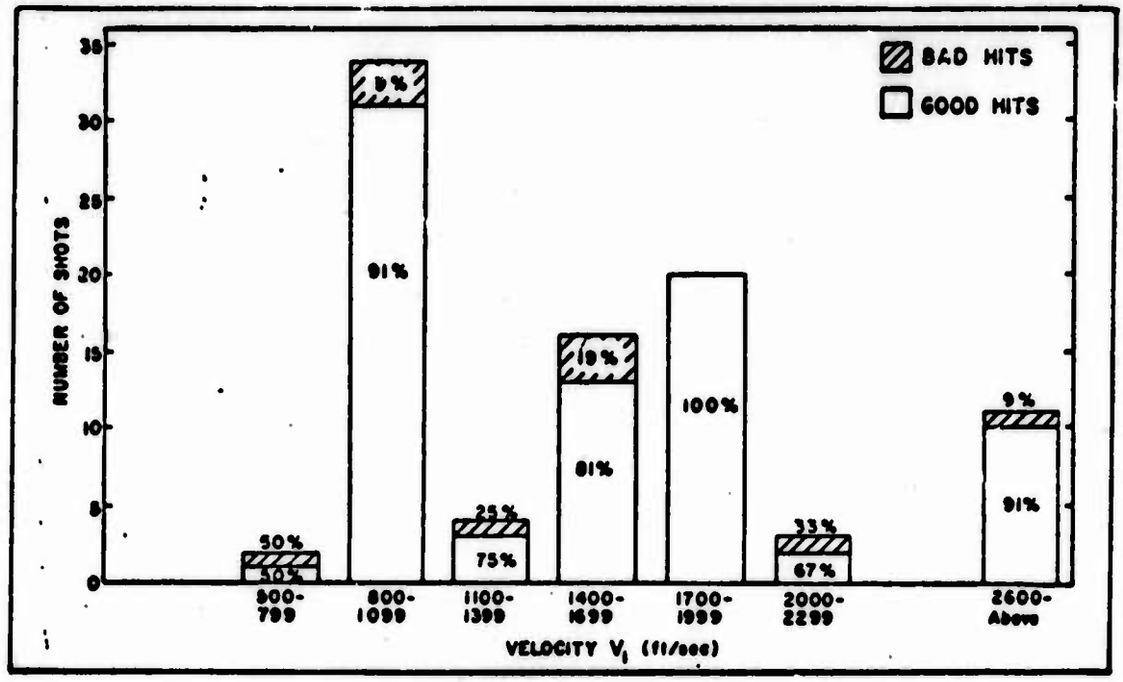

Fig. 6. Flat-Launched Cube Success Rates

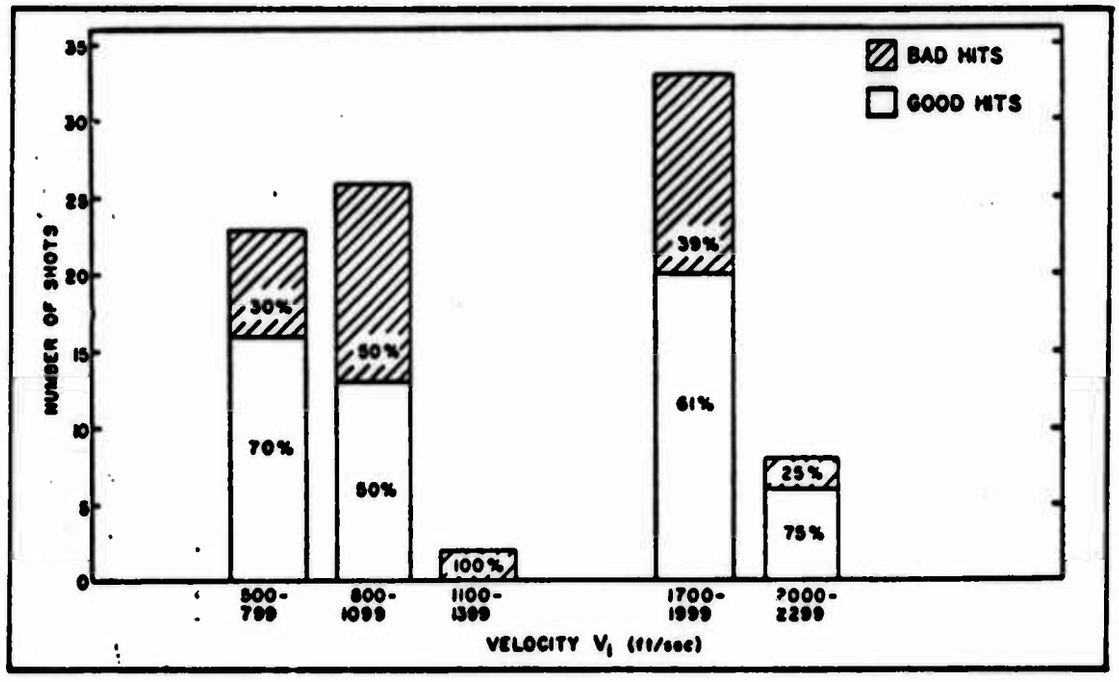

Fig. 7. Edge-Launched Cube Success Rates

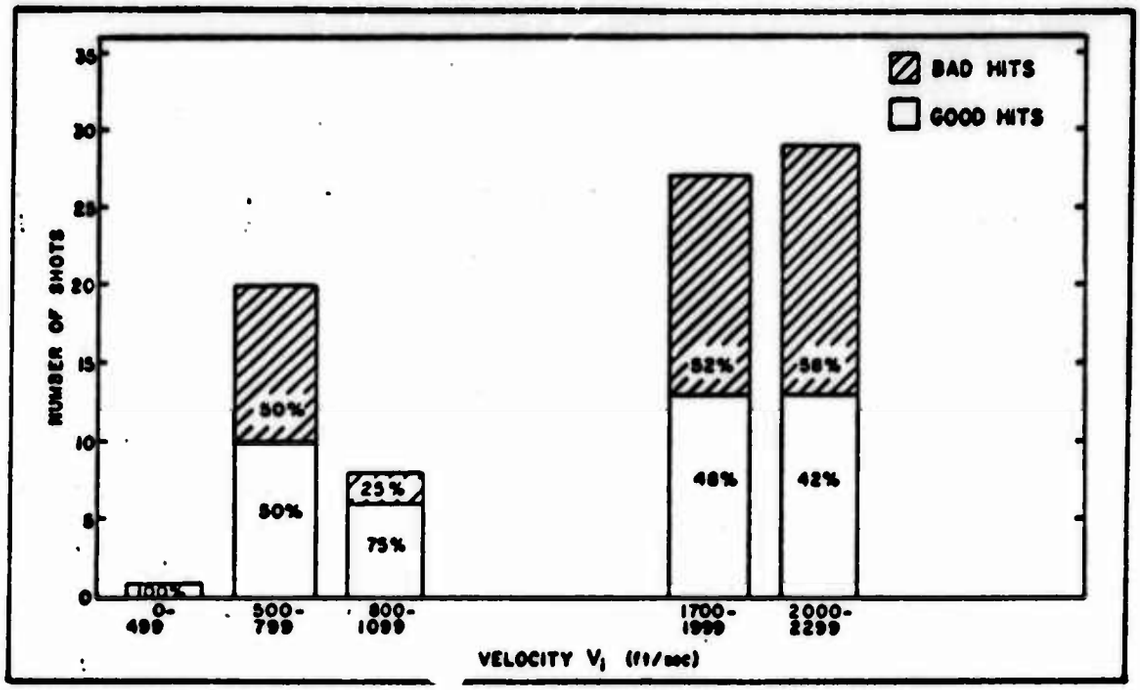

Fig. 8. Point-Launched Cube Success Rates

percentage of the shots would be successful. The concept of the error angles introduced in Section II allowed all the shots in the series to be used for the ballistic limit study.

Yaw cards were used to determine the orientation of the cubes at impact. Opposite parallel edges of the perforation silhouette were measured to three significant figures with a Gaertner micro-slide comparator and the average value for each pair of edges was used to compute the impact angles.

The impact angles were computed from Eqs (6), (7), (8), (9), and (10). When the three error angles are equal, that is, no predominant orientation, the three impact angles are $\theta = 16.4^{\circ}$, $\phi = 21.5^{\circ}$, and $\epsilon = 62.4^{\circ}$. The standard cube edge dimensions of 0.250 inch were used in all calculations of impact angles, rather than the actual cube

dimensions of 0.250 ± .003 inches. The error introduced by this assumption allowed the no-predominant-orientation impact angles to vary as follows:

$$12.5^\circ < \theta < 18.6^\circ$$
$$19.7^\circ < \phi < 23.2^\circ$$
$$62.1^\circ < \epsilon < 62.8^\circ$$

Ballistic Limits of Selected Armor Materials

Table IIa gives the overall results of the V_{50} ballistic limit testing program. Tables IX-XX in Appendix D give the tabulated results of the V_{50} ballistic limit testing.

Figs. 9a, 9b, 9c, and 9d provide a comparison of cube presented area versus the impact velocity for the four materials. The dashed line represents the estimated boundary between complete and partial penetrations, thus the ballistic limit of the materials for varying presented areas. With the exception of the flat impact for the layered nylon (Fig. 9d), the ballistic limits (Table IIb) are in close agreement with values listed in Table IIa.

Examination of the data points reveal that the presented area is not the controlling factor in ballistic limits determined with cubes. Rather, it is the shape factor or geometry of the impacting cube.

It should be noted that this method of ballistic limit determination gives a much better indication than the flat-edge-point concept of the V_{50} determination, of the actual ballistic limits of the material.

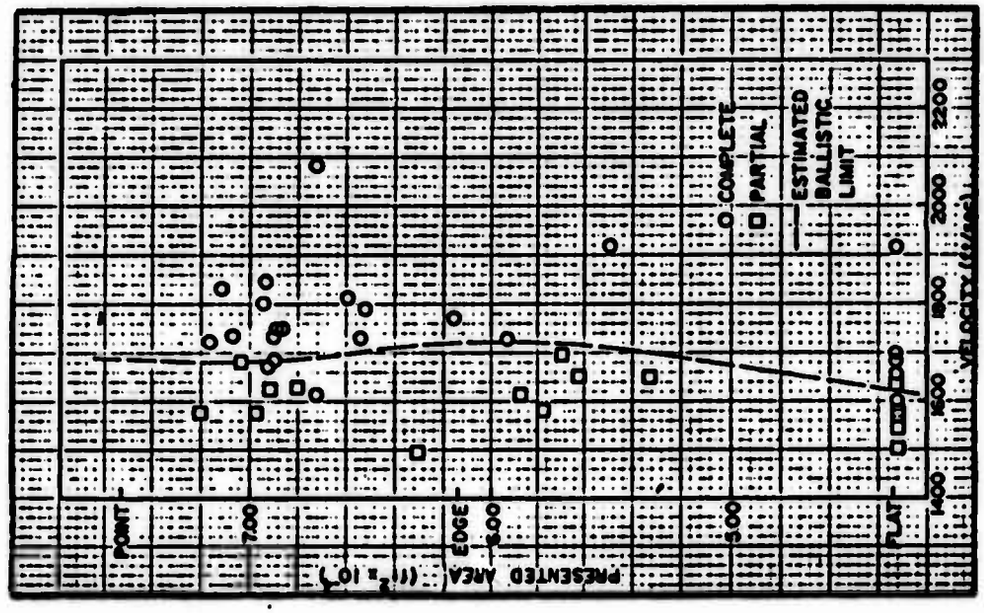

b. Steel Plate (0.125 inch)

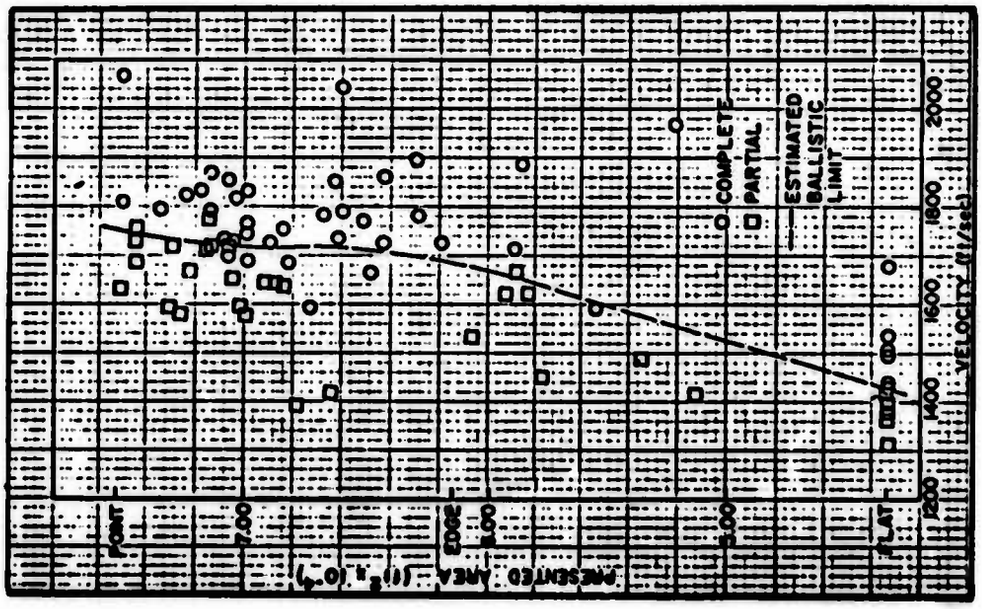

a. Aluminum Plate (0.250 inch)

Fig. 9. Impact Velocity vs. Presented Area

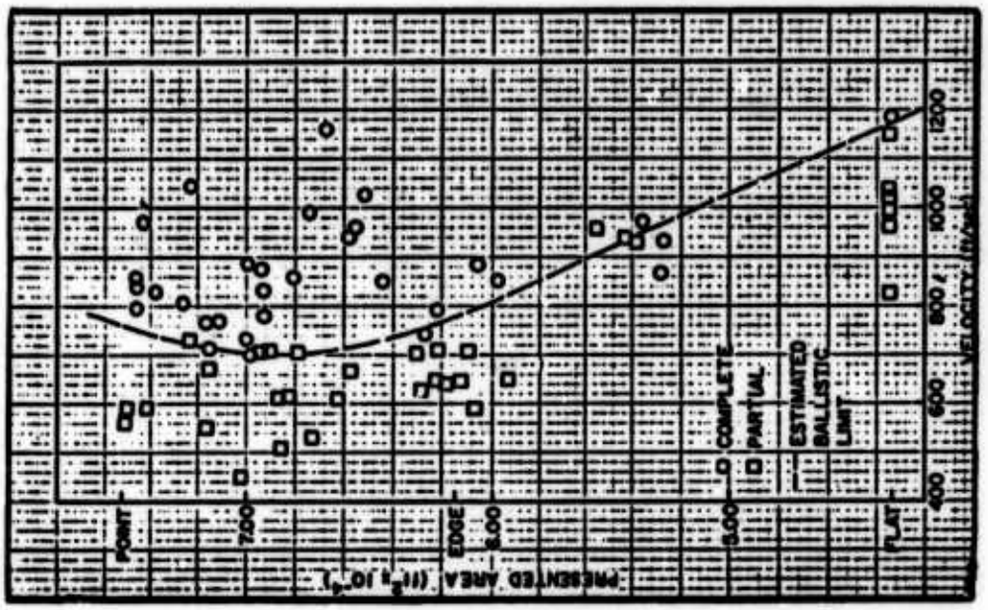

d. Unbonded Nylon (12-layer)

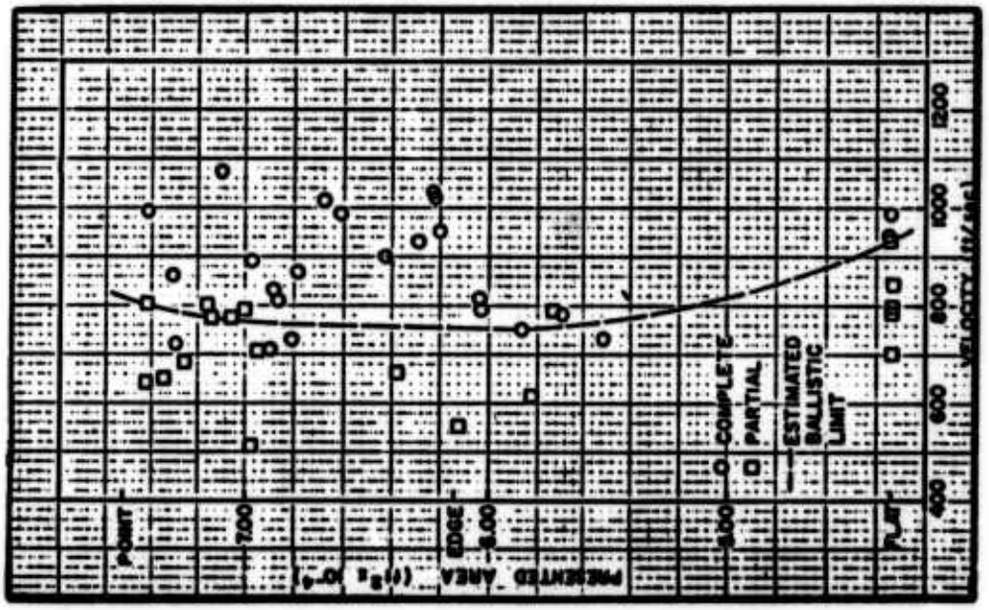

c. Ballistic Felt (0.5 inch)

Fig. 9. Impact Velocity vs. Presented Area

Table IIa

V_{50} Ballistic Limits of Selected Armor Materials

	2024 T-351 Aluminum (0.250 inch)	1030 Hot-Rolled Steel (0.125 inch)	Ballistic Felt (0.5 inch)	Ballistic Nylon (12-layer)
Flat	1470	1632	911 (8)	998 (8)
Edge	1701	1693	748	721 (8)
Point	1765	1719 (6)	760 (2)	738 (8)

* Note: All velocities are in ft/sec. ( ) indicates ten shot series not obtainable.

Table IIb

Ballistic Limits of Selected Armor Materials
Based on Presented Area at Impact

	2024 T-351 Aluminum (0.250 inch)	1030 Hot-Rolled Steel (0.125 inch)	Ballistic Felt (0.5 inch)	Ballistic Nylon (12-layer)
Flat	1430	1620	930	1170
Edge	1685	1720	755	775
Point	1755	1685	815	760
Minimum	1430	1620	750	700

A better approach than the V_{50} method might be to take the lowest velocity value on the ballistic limit curve and establish a 50 ft/sec band on either side of this point with the requirement for at least five complete and five partial penetrations to lie within this band.

In some cases, a ten shot V_{50} ballistic limit could not be established. This was especially true in the case of the point impacts, where the success rate was low enough to require an excessive number of shots.

at velocities above the ballistic limit, the shearing becomes less significant (Ref 14:29).

The range of ballistic limits for the three cube orientations impacting the thinner steel plate is smaller than was observed during the aluminum impacts. In this case, the point and edge impacts had nearly penetrated the plate before the shearing forces on the cube perimeter reached a maximum. Cube deformation was noted for all cases of steel impacts, with edge and point impacts exhibiting the greatest deformation. Little or no deformation was noted for cube impacts against the aluminum target.

The non-homogeneous materials, such as ballistic felt and layered nylon, exhibited ballistic limit velocities that were higher for the flat impacts and lower for the edge and point impacts. It is theorized that, during flat impact, energy was absorbed by the stretching of the fabrics before rupture, whereas, the edge and point impacts cut and separated the fibers as the cube passed through the material.

Figs. 10a and 10b are plots of ballistic limits obtained by Cressmer (Ref 4:22-26) using the standard fragment-simulators to evaluate one-quarter inch 24S-T Aluminum plate and layered (unbonded) nylon. He used the standard .15, .22, .30, .45, and .50 caliber fragment-simulators with the masses of the projectiles ranging from 5.8 grains to 207 grains. A comparison of the 31 grain cube ballistic limits show a higher ballistic limit value for the aluminum and a lower ballistic limit value for the nylon than Cressmer obtained with the

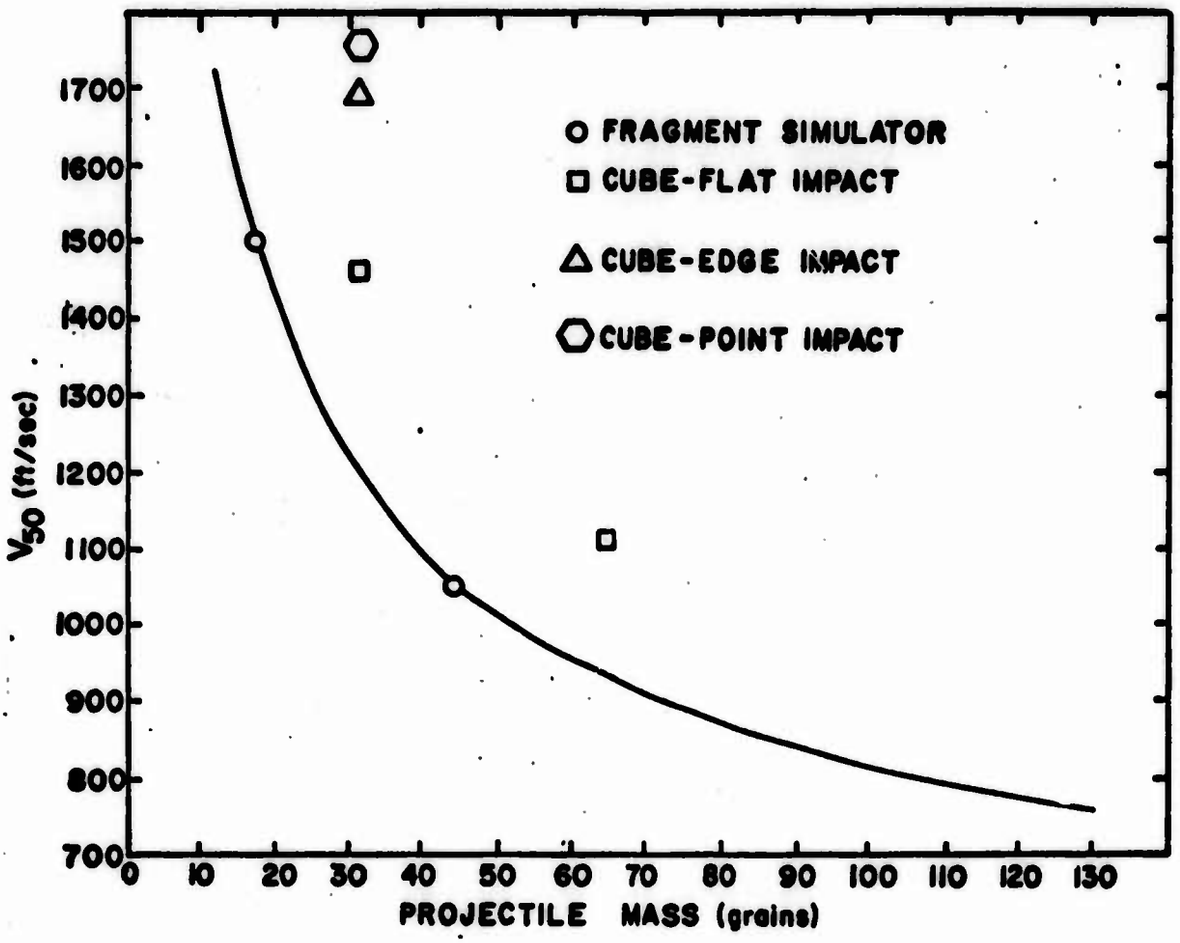

Fig. 10a. Ballistic Limits of 0.250 inch Aluminum Plate Using Fragment-Simulating Projectiles and Cubes

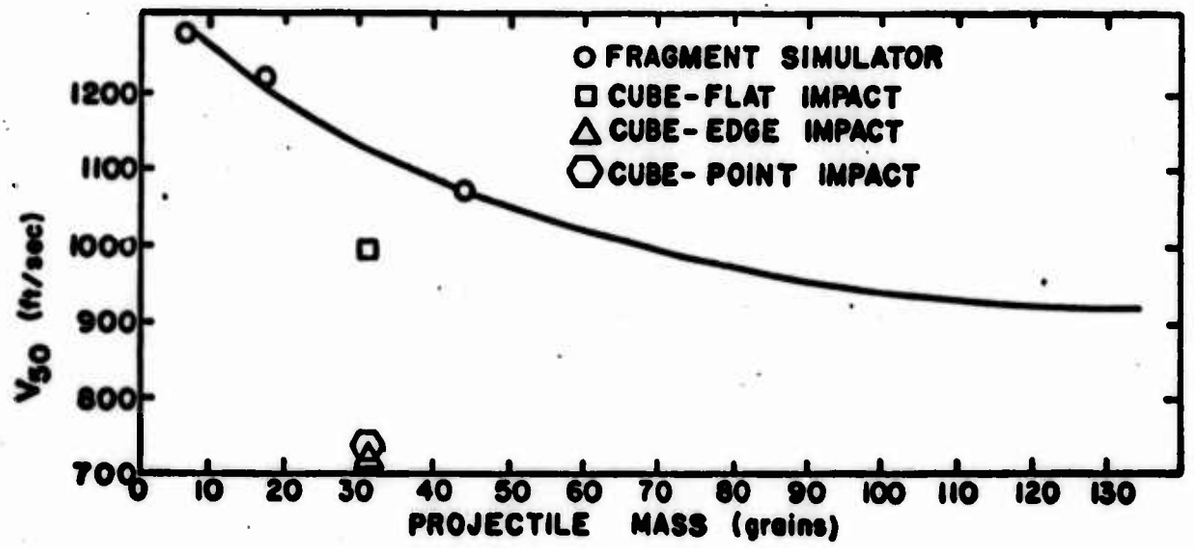

Fig. 10b. Ballistic Limits of 12-Layer Unbonded Nylon Using Fragment-Simulating Projectiles and Cubes

fragment-simulators. The JIBAC study obtained a ballistic limit against 2024-T351 Aluminum plate of 338.6 meters per second (1111 ft/sec) for 64 grain cubes (Ref 27:17). The cubes were launched in a predominantly flat orientation, and approximately 72% of the cubes impacted in a predominantly flat orientation with no attempt made to control the orientation of the cube. This indicates that, for the materials tested, the fragment-simulator is a more efficient penetrator against homogeneous materials than cubes, but are less efficient against the non-homogeneous fiber materials.

A comparison was made between the change in momentum per unit area $\frac{m\Delta v}{A}$ for the flat-faced cube impact and the fragment-simulator impact. Only the flat face area of the fragment simulator was considered in the calculation. Assuming that the projectile velocities went to zero at impact, that is, all momentum was transferred to the plug, it was seen that the net momentum transfer per unit area for the cubes (both 31 and 64 grain) were only 60% of the net momentum transfer per unit area for a simulator of equivalent mass, thus giving higher ballistic limit values for the cube impact.

An attempt was made to correlate the ballistic limit data for cubes with the penetration model of Heyda (Ref 11). Heyda investigated the penetration of thin aluminum and steel plates by steel cylinders. However, the critical factor in Heyda's model is the target thickness to projectile length ratio. His theoretical model does not hold for a ratio in the range of 0.5 or greater. Neither of the homogeneous targets satisfied this criteria.

Determination of Drag Coefficients

Figs. 11, 12, and 13 on the following pages illustrate the variation of C_D with Mach Number for the three cube orientations. The complete results are tabulated in Table VI-VIII in Appendix D.

The general shape of the drag curves was determined by the superposition of all the data points from the three launch orientations. It was assumed that the shape of the curve was the same for all orientations.

In the calculation of C_D, it was assumed that the cube presented area ta launch remained constant throughout the trajectory and the data points in Figs. 11, 12, and 13 reflect this assumption. The solid lines are the drag curves based on this assumption and the actual measured cube presented areas at launch.

The standard cube presented area for the flat orientation may vary from 4.34×10^{-4} ft^2 (perfect flat orientation) to 6.68×10^{-4} ft^2 (no predominant orientation, i.e., all three error angles equal). Likewise, the edge-orientation presented area (Fig. 12) may vary from 5.57×10^{-4} ft^2 to 7.16×10^{-4} ft^2 and the point-orientation presented area (Fig. 13) may vary from 6.68×10^{-4} ft^2 to 7.53×10^{-4} ft^2 (perfect point orientation). The dashed lines indicate the limits of C_D for the variance in presented area.

The lower limits of C_D, based on the maximum presented area for the flat orientation (Fig. 11) lie near the lower limits of the figure.

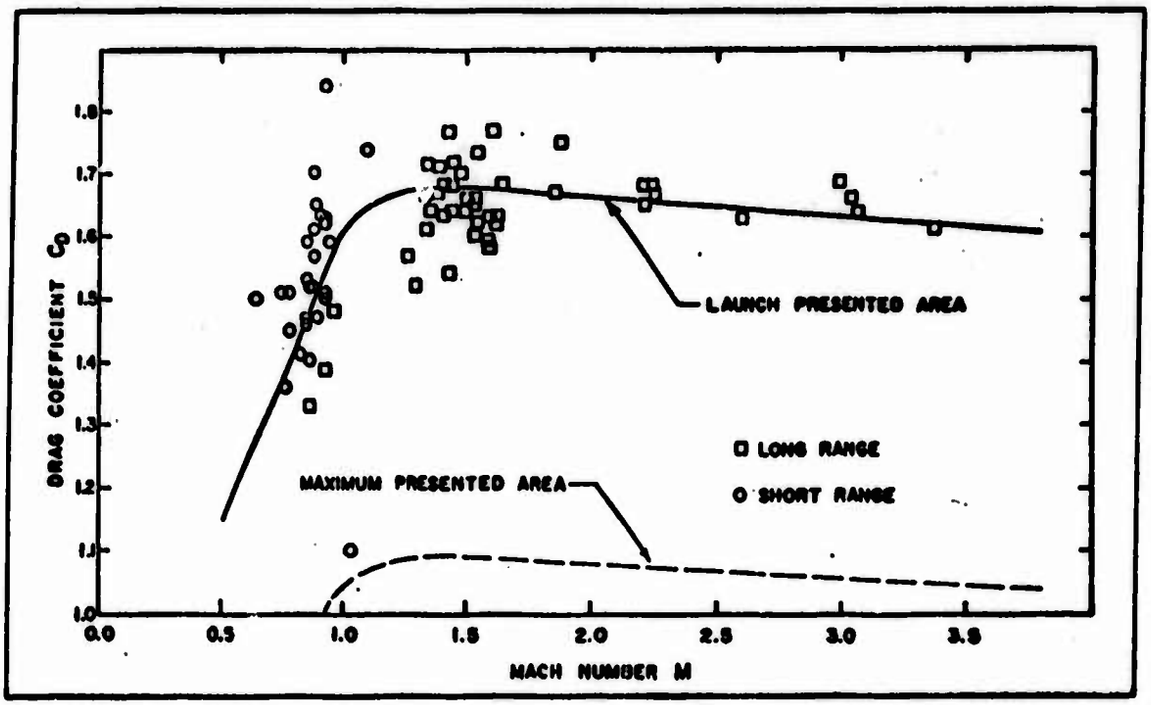

Fig. 11. C_D vs. Mach Number - Flat Orientation

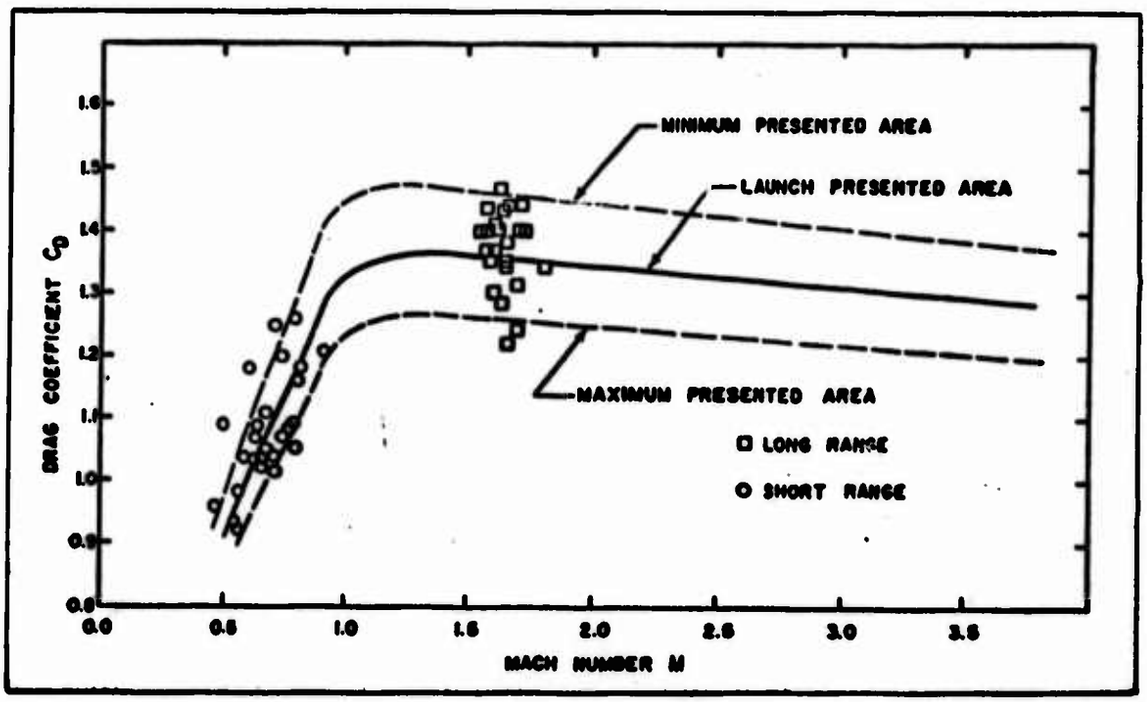

Fig. 12. C_D vs. Mach Number - Edge Orientation

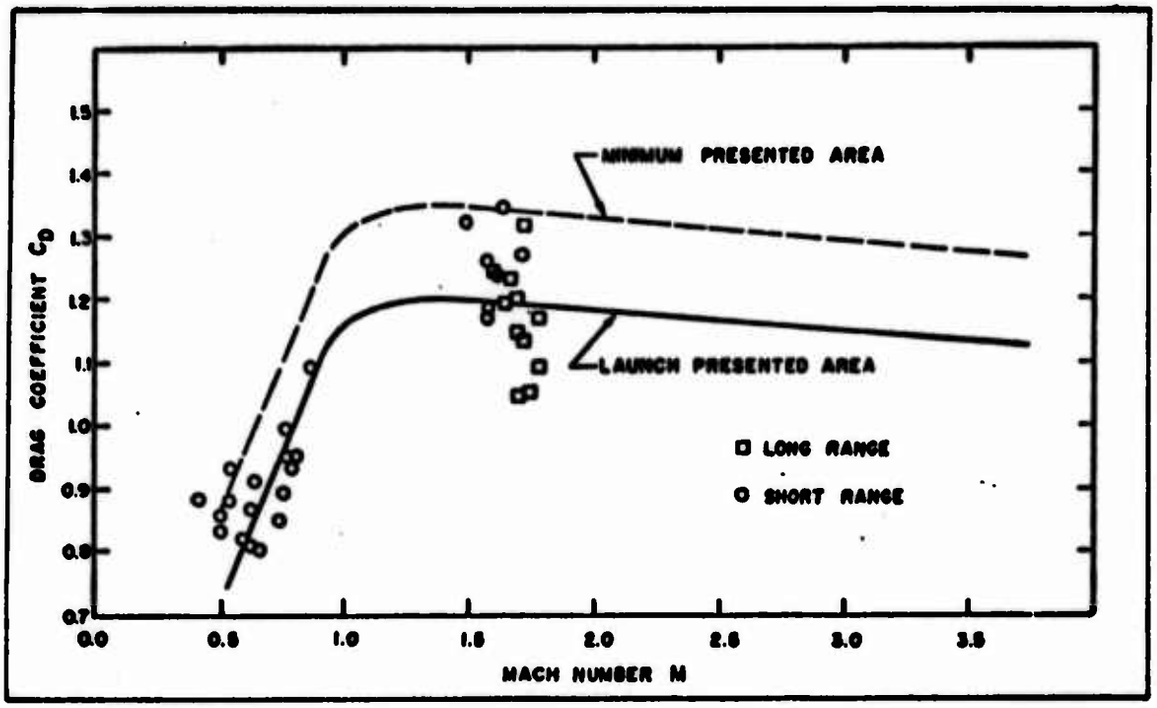

Fig. 13. C_D vs. Mach Number - Point Orientation

The high percentage of perfect flat impacts (57%) and the overall success rate (89%), indicated that the cubes were quite stable in the flat orientation, hence the large possible variation in presented area was ignored.

The drag curves reveal that the coefficient of drag is greatest for the flat orientation and least for the point orientation. The drag force, D, which is a function of the product of C_D and A, is greatest for the point orientation. It would seem logical to assume that the cube would tend to fly at this orientation of maximum drag. However, the experimental results show that this is not the case.

This anomaly can best be explained by observing how the center of aerodynamic pressure affects the flight of the cube. During point-forward flight orientation, the center of pressure slips across the three

forward faces of the cube as it spins, hence the cube is not stable, but gyrates continually as the center of pressure shifts.

The center of aerodynamic pressure on the edge orientation shifts between only two planes, which causes the cube to rock about the leading edge and retain some degree of stability.

The center of pressure on the flat orientation moves freely about the leading face, but rarely goes off the face. Thus, the flat orientation is the most stable, despite the lowest drag force of the three orientations.

The twist calculations using the Hansche and Rhinehart data was compared to the experimental data of this study. The maximum value of C_D and presented area for each of the three predominant orientations was taken from Figs. 11, 12, and 13, and substituted into Eq (14), Appendix C. The following values of C_DA were used:

$$C_DA\,(\text{Flat}) = 7.31 \times 10^{-4}\ \text{ft}^2$$

$$C_DA\,(\text{Edge}) = 8.37 \times 10^{-4}\ \text{ft}^2$$

$$C_DA\,(\text{Point}) = 9.04 \times 10^{-4}\ \text{ft}^2.$$

The required twists were computed:

Twist (Flat) = one turn in 39.6 in.

Twist (Edge) = one turn in 31.2 in.

Twist (Point) = one turn in 27.1 in.

The influence of the velocity screens on cube stability needs to be considered. It was noted that, in almost all instances, the velocity screen perforation silhouettes were consistent with the impact silhouette.

Shots that were bad initially (at the first velocity screen) were consistently bad impacts. If the cube passed through the velocity screens in its launch orientation, the impact silhouette was equally consistent. It is felt that the velocity screens may have had some influence on cube stability, but a more critical consideration was the cube-sabot separation.

The sabot fit into the barrel was necessarily tight so that maximum spin effect could be derived from the rifling. The cube-sabot fit was also snug so that the cube would not fall out of the sabot during insertion into the barrel. Examination of the sabot impact pattern in the sabot catcher showed that the cube-sabot separation was not always symmetrical. It was felt that, in these cases, the tight fit and squeezing effect of the barrel caused the cubes and sabots to stick together long enough to perturb the cube orientation. Several sabots were recovered with definite cube impressions in the pockets.

This study has not been able to definitely answer the basic question of cube spin-stabilization. The preliminary testing definitely demonstrated that it is possible to overspin the cube and destroy the trajectory, while smoothbore launchings were not acceptable due to insufficient sabot separation. The method presented in this study provides positive sabot separation, adequate trajectories, and acceptable cube impact orientation predictability. However, it is not clear whether the improvement in orientation predictability was due to spin stabilization of the cube or due to cleaner separation characteristics of the sabot as a result of the spin.

V. Conclusions and Recommendations

Conclusions

While the launch method used in this study is not presently 100% effective in achieving desired cube impact orientation, it has been shown that an acceptable level of success has been achieved by launching the cube-sabot combination from a rifled barrel.

This study has demonstrated the basic feasibility of using cubes as fragment-simulators. While the standard fragment-simulators are a more efficient penetrator of homogeneous materials and thus give lower ballistic limit velocities than cubes of the same mass, hence, better protection criteria; the use of these projectiles against fibrous materials does not give a reliable indication of their resistance to penetration. The results of this study show that ballistic limits are dependent on cube orientation but are independent of presented area.

V_{50} ballistic limits can be determined for each of the three predominant cube orientations and this information used to define the protection criteria for various armor materials. An alternate approach is to define the ballistic limit by considering the minimum penetration velocity under all orientations.

The drag data of Hansche and Rhinehart (Ref 9) is only valid for cubes with point orientation. The flat orientation product, C_DA, obtained in this study is considerably less than the C_DA product determined by Hansche and Rhinehart (See Fig. 2).

The present method of low velocity launching results in many wasted shots because of the erratic velocity behavior. Velocity variations of 200 ft/sec with identical powder loads were not uncommon.

Recommendations

The following recommendations are based on the results and experimental methods of this study:

a. Additional armor materials should be evaluated with cubes and comparisons made with the standard fragment-simulator data.

b. Consideration should be given to the adoption of the ballistic limit method for cubes discussed in this study in lieu of the current V_{50} standard.

c. A system should be designed for launching the sabot in a conventional manner to provide better velocity control at velocities below 1000 ft/sec. Pressing the sabots into the casings should solve part of this problem.

d. Further testing should be done with a barrel with a twist of one turn in 20-22 inches to examine cube-sabot separation and cube stability.

e. Further experimentation with the sabot pocket design should be considered to achieve better cube-sabot separation.

f. A "soft" velocity measuring system should be developed to avoid possible perturbation of the cube orientation by velocity screen penetration.

g. The motion of the cube in flight should be studied with sequence photography. Cubes could be marked with various designs on the faces to study their stability.

h. Studies should be conducted with cubes launched in a vacuum to determine if aerodynamic forces have any effect on cube stabilization.

i. Additional drag studies should be conducted in the Mach 2.0 to 4.0 velocity range.

Bibliography

1. Bertke, R.S. The Air Force Materials Laboratory Terminal Ballistic Research Facility. AFML-TR-69-215. Wright-Patterson Air Force Base, Ohio: Air Force Materials Laboratory, October 1969.

2. Charters, A.C. and R.N. Thomas. "The Aerodynamic Performance of Small Spheres from Subsonic to High Supersonic Velocities." Journal of the Aeronautical Sciences, 12:468-76 (October 1945).

3. Clark, A.B.J. and F.T. Harris. "Free-Flight Air-Drag Measurement Techniques." Journal of the Aeronautical Sciences, 19:385-90 (June 1952).

4. Cresmer, H.M. Jr. Report on a Test of Personnel Armor Materials with Fragment-Simulating Projectiles. Armor Test Report AD-1190. Aberdeen Proving Ground, Maryland: Development and Proof Services, February 1954.

5. Cummings, C.S. Everyday Ballistics. Harrisburg, Pennsylvania: Stackpole and Heck, Inc., 1950.

6. Dunn, D.J. Jr. and W.B. Porter. Air Drag Measurements of Fragments. BRL MR-915. Aberdeen Proving Ground, Maryland: Ballistic Research Laboratories, August 1955.

7. Ewing, W.O. Jr. The Design and Function of a Sabotless-Type Fragment Launcher. BRL TN-1117. Aberdeen Proving Ground, Maryland: Ballistic Research Laboratories, April 1957.

8. Greenwood, E.W. and J.J. Maroney. Correction for Card Effect in the Yaw Card Determination of Stability Factor of Gun Shell. CARDE-TM AB-50. Valcartier, Quebec: Canadian Armament Research and Development Establishment, March 1958.

9. Hansche, G.E. and J.S. Rhinehart. "Air Drag on Cubes at Mach Numbers 0.5 to 3.5." Journal of the Aeronautical Sciences, 19:83-4 (February 1952).

10. Heppner, L.D. and J.E. Steedman. Drag Coefficient for Fragment-Simulating Projectiles, 20 MM, Caliber .50 and Caliber .30. DPS Report 286. Aberdeen Proving Ground, Maryland: Development and Proof Services, August 1961.

11. Heyda, J.F., et al. A Combined Theoretical and Experimental Investigation of Armor Penetration Mechanics. AFATL-TR-70-78. Eglin Air Force Base, Florida: Air Force Armament Laboratory, August 1970.

12. Hodges, A.J. "The Drag Coefficient of Very High Velocity Spheres." Journal of the Aeronautical Sciences, 24:755-58 (October 1957).

13. Ipson, T.W. Ballistic Perforation Performance of a Specified Preformed Fragment. NWC TP-4755. China Lake, California: Naval Weapons Center, September 1970.

14. -----. Deformation and Reduction in Weight of Compact Steel Fragments Perforating Thin, Mild Steel Plates. NWC-TP-4533. China Lake, California: Naval Weapons Center, January 1968.

15. Jones, D.H. The Properties and Performance of Fragments. Dahlgren, Virginia: Naval Weapons Laboratory, November 1967.

16. Karpov, B.G. A Comparison of Aerodynamic Data Obtained By "Yaw Card" and Spark Photography Methods. BRL-MR-728. Aberdeen Proving Ground, Maryland: Ballistic Research Laboratories, October 1953.

17. Kelly, J.L. and E.J. McShane. On the Motion of a Projectile with Small or Slowly Changing Yaw. BRL Report 446. Aberdeen Proving Ground, Maryland: Ballistic Research Laboratories, January 1944.

18. Kent, R.H. Notes on a Theory of Spinning Shell. BRL Report 898. Aberdeen Proving Ground, Maryland: Ballistic Research Laboratories, February 1954.

19. Kent, R.H. and E.J. McShane. An Elementary Treatment of the Motion of a Spinning Projectile About Its Center of Gravity. BRL Report 459. Aberdeen Proving Ground, Maryland: Ballistic Research Laboratories, April 1944.

20. Krafft, J.M. "Surface Friction in Ballistic Penetration." Journal of Applied Physics, 26:1248-53 (October 1955).

21. May, A. and W.R. Writt, Jr. "Free-Flight Determination of Drag Coefficients of Spheres." Journal of the Aeronautical Sciences, 20:635-38 (September 1953).

22. Meriam, J. L. Mechanics-Part II Dynamics (Second Edition). New York: John Wiley and Sons, Inc., 1959.

23. Muldoon, R.A. Determination of Coefficient of Drag, K_D, and Development of Velocity Loss Equation for the Fragment-Simulating Type Projectiles Used to Evaluate Personnel Armor Materials. WAL Report 760/503. Watertown, Mass.: Watertown Arsenal, January 1953.

24. Prescott, J. Mechanics of Particles and Rigid Bodies (Third Edition). New York: Longmans, Green and Co., 1929.

25. Shaw, J.E. A Measurement of the Drag Coefficient of High Velocity Fragments. BRL Report 744. Aberdeen Proving Ground, Maryland: Ballistic Research Laboratories, October, 1950.

26. Synge, J.L. and B.A. Griffith. Principles of Mechanics. New York: McGraw-Hill Book Co., Inc., 1949.

27. Van Caneghem, R.J. and W.C. Pless. Special Study of Body Armor, Joint Operational Requirement (Reliability in Ballistic Test Procedures and Test Results). APG-MT-3497. Aberdeen Proving Ground, Maryland: Aberdeen Proving Ground, April 1970.

28. Warnis, R.P. Penetration of 15-Grain Bomb Fragments into Wallboard. AFATL-TR-70-18. Eglin Air Force Base, Florida: Air Force Armament Laboratory, February 1970.

29. Whiteford, C.W. and J.M. Regan. The Determination of the Striking Velocity of Steel Fragments by Their Mass and Penetration into Witness Material. BRL-MR-1333. Aberdeen Proving Ground, Maryland: Ballistic Research Laboratories, April 1961.

30. Zaroodny, S.J. A Simplified Approach to the Yawing Motion of a Spinning Shell. BRL Report 921. Aberdeen Proving Ground, Maryland: Ballistic Research Laboratories, August 1954.

Appendix A

Description of Equipment

The Air Force Materials Laboratory Terminal Ballistic Facility, located in Buildings 44 and 56, Area B, at Wright-Patterson Air Force Base, Ohio, was used for all testing in this study. The ranges are operated by the University of Dayton Research Institute under Air Force contract.

The Fragment Simulation Facility, located in Building 56, was used for the early part of this study to determine the feasibility of preferred orientation cube launches (Ref 1:14). Range Number One of the Conventional Projectiles Facility, located in Building 44, was used for the drag and ballistic limit studies (Ref 1:7). The range equipment consisted of the gun, sabot catcher, velocity measurement system, yaw cards, and photographic system. Fig. 14 illustrates the range layout.

Gun

The gun used was a .50 caliber barrel rifled for one revolution per 28 inches of projectile travel. The 48 inches long barrel was mounted on a steel I-beam by means of two yoke-type pipe vises with the jaws modified to hold the barrel. The barrel was shimmed to align its optical axis with the target. The 300 H and H Magnum casings were loaded with Hercules Unique powder and percussion fired by a remote control electric solenoid. Fig. 15 illustrates the gun configuration.

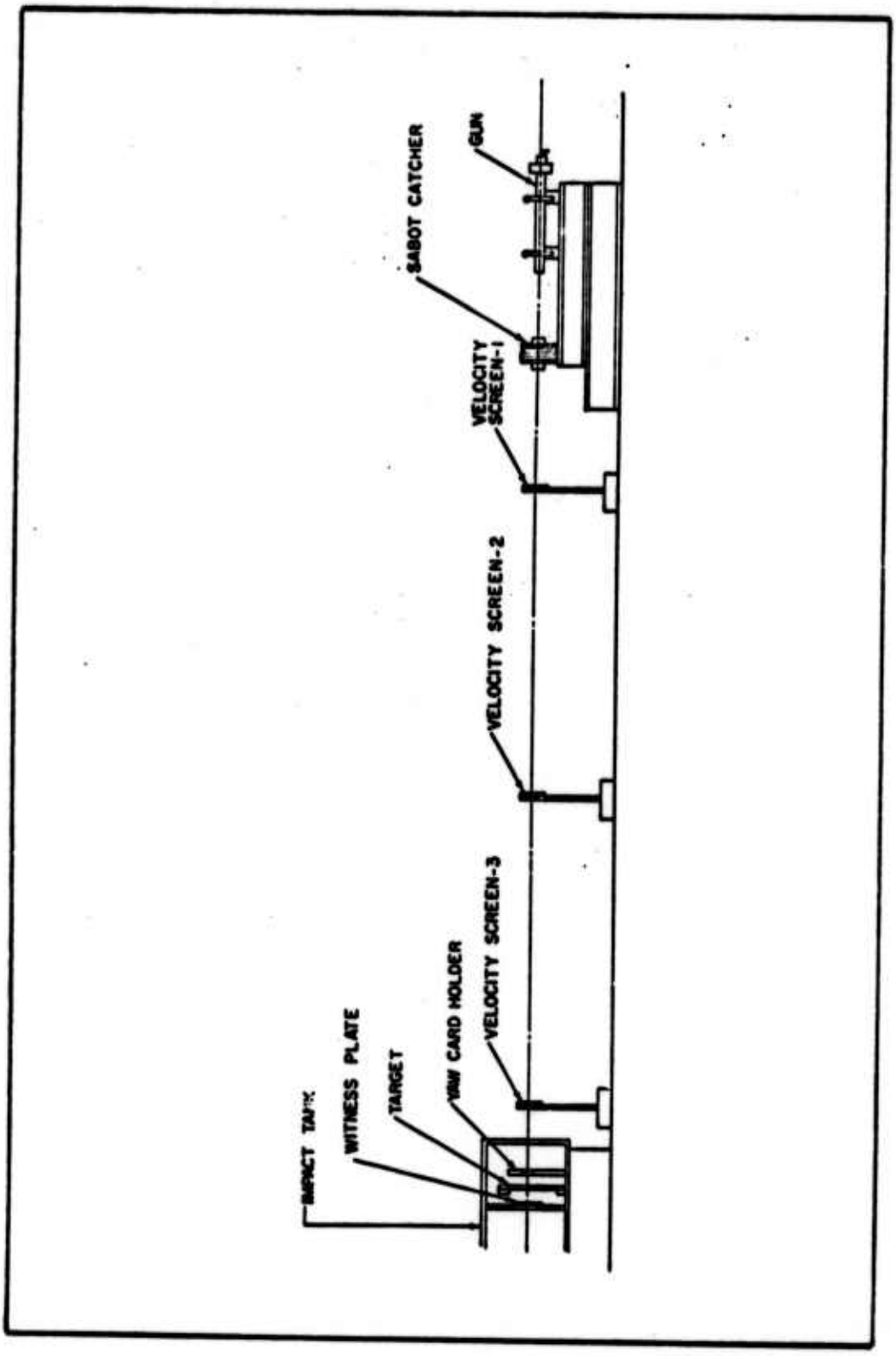

Fig. 14. Range Layout

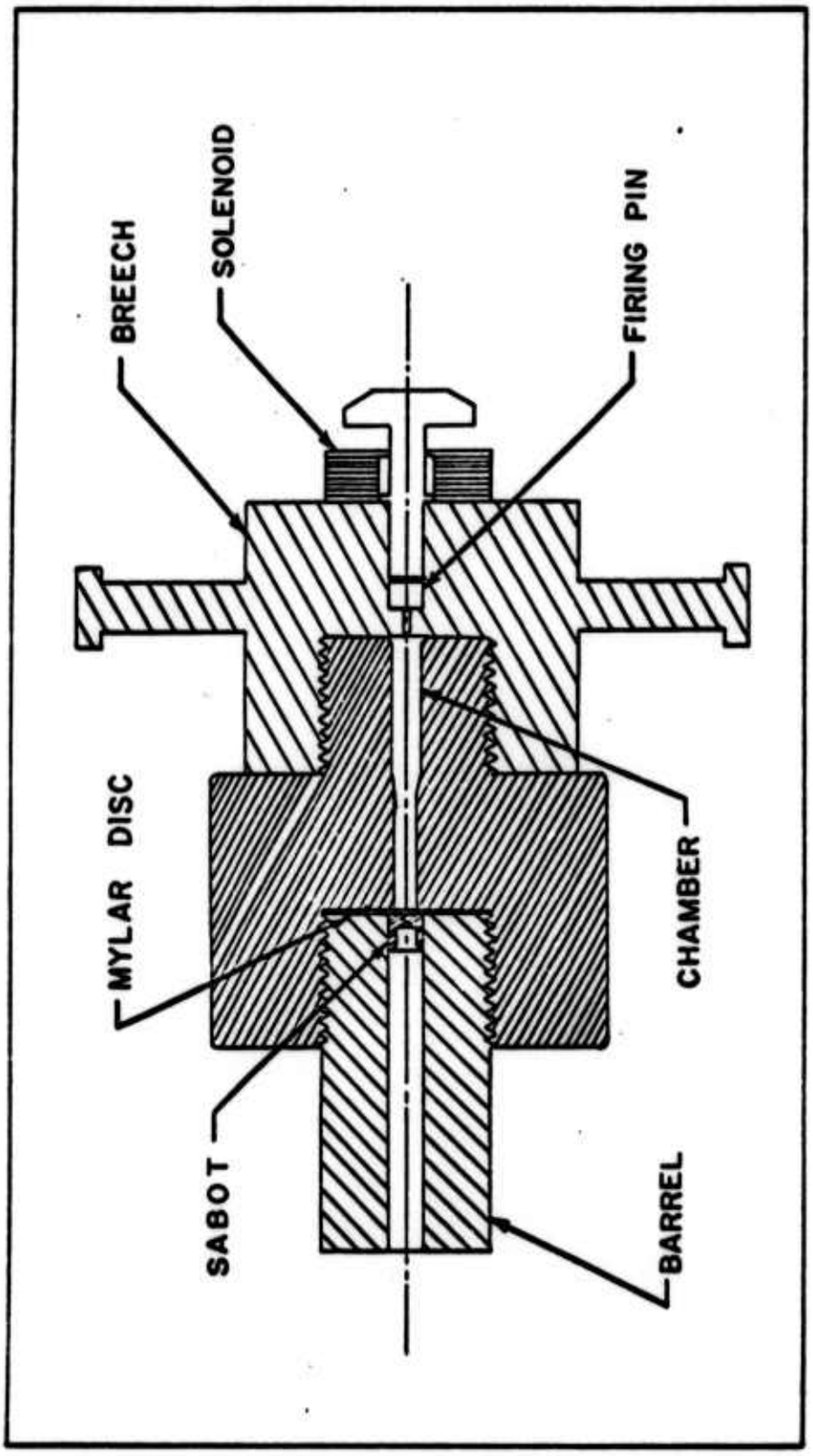

Fig. 15. Gun Used to Launch Cubes

Sabot Catcher

A 20" x 23" x 7" wooden frame packed with several layers of one-half inch thick ballistic felt was used as a sabot catcher. The frame was placed six feet from the gun muzzle. The center portion of the frame was removed and a four inch diameter steel pipe was inserted to provide additional separation for the sabot pieces and to prevent velocity screen contamination by the sabot pieces.

Velocity Screens

The velocity screens were composed of 0.5 mil (0.0005 inch) mylar sandwiched between two sheets of 0.5 mil (0.0005 inch) aluminum foil. A potential of 600 volts was applied across the screens, which triggered an electric pulse when the screens were perforated by the projectile.

Chronographs

Projectile velocities were determined by measuring the time required to traverse the distance between three velocity screens, which were placed twelve feet apart on the long range and five feet apart on the short range. Perforation of velocity screen Number 1 started the Eldorado Electronics Model 1410-R5 Universal Counter Timer. Perforation of velocity screen Number 2 stopped the Eldorado Counter and started the Beckman Universal EPUT and Timer, Model 7360A. Perforation of velocity screen Number 3 stopped the Beckman timer.

Yaw Cards

Standard photographic print paper was used for the yaw cards. The cards were placed five inches in front of the target material, with the emulsion side facing the gun. The impacting cube shears the emulsion from the paper leaving a perfect silhouette of the cube orientation at impact. Yaw cards were also placed in the velocity screen holders to study cube orientation along the flight trajectory during the initial testing.

Photographic System (Ref 1:12)

Impact orientation photographs were made with a Burke and James View Camera, operated in the "open shutter" mode, and a Beckman and Whitley Model 5403 Dual Flash Lamp. A Polaroid magazine was mounted on the back of the camera. The flash lamps were of one microsecond duration and were triggered by perforation of velocity screen Number 3. Sabot separation photographs were also made with the above equipment. The triggering system was provided by photo-electric cells positioned at the gun muzzle.

Appendix B

Description of Lexan Sabots

Lexan sabots were designed by the University of Dayton Research Institute and manufactured by Browder Industries of Dayton, Ohio. Fig. 16 illustrates the overall dimensions of the unpocketed sabot. Three types of sabots were molded to hold the cubes in each of the three preferred launch orientations.

Two sabots were cut from each unfinished sabot unit. The length of the serrated section was found to be extremely critical for good sabot separation. Numerous modifications were performed on the sabots before arriving at the final finished configuration in Figs. 17, 18, and 19. The sabots were turned on a lathe to the dimensions noted.

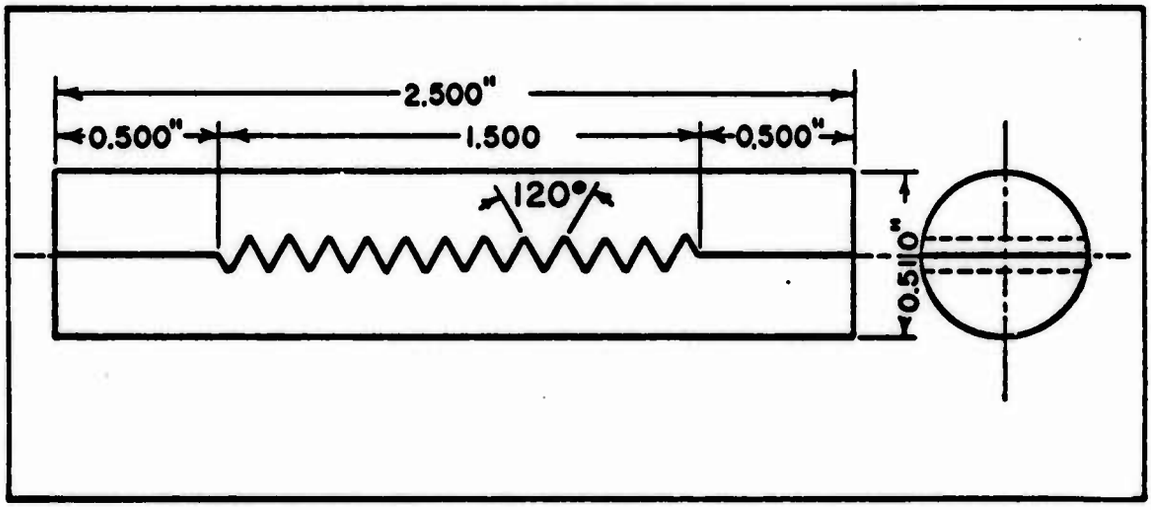

Fig. 16. Unpocketed Launch Sabot

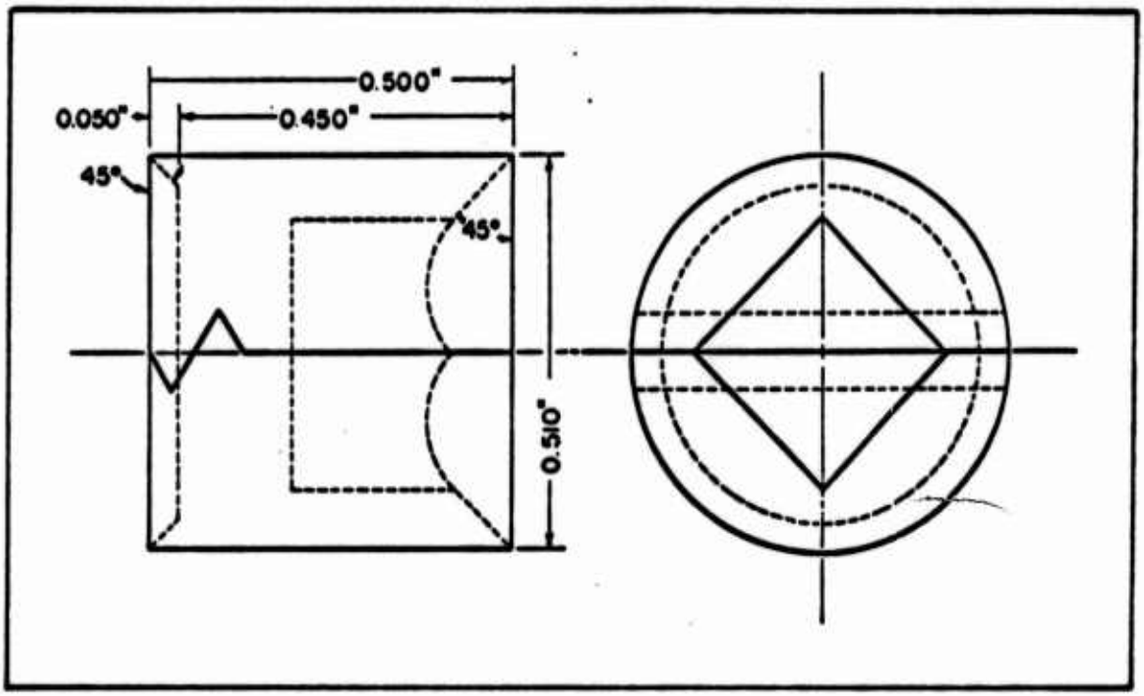

Fig. 17. Flat-Launched Cube Sabot Configuration

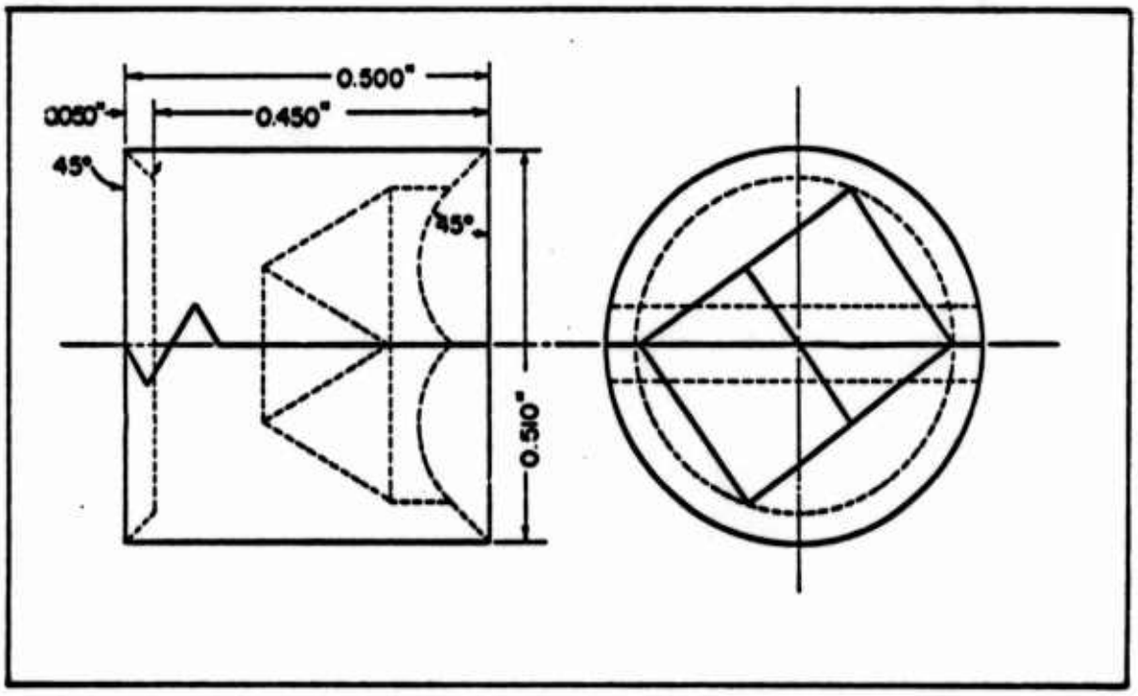

Fig. 18. Edge-Launched Cube Sabot Configuration

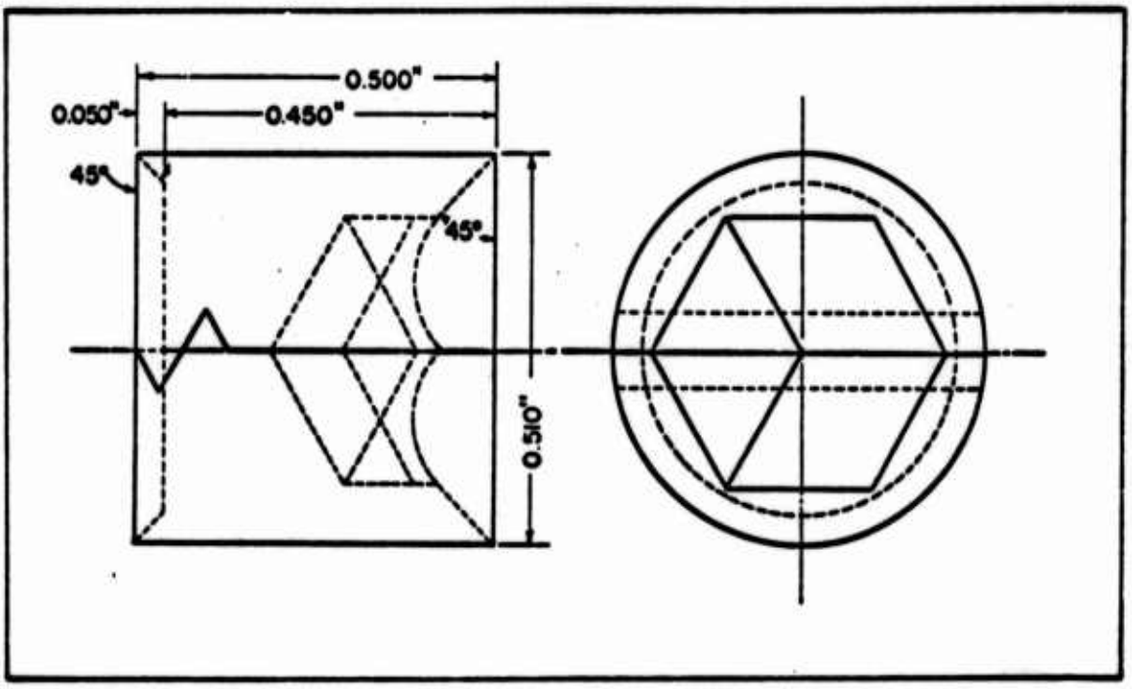

Fig. 19. Point-Launched Cube Sabot Configuration

All rough edges and corners were removed with a knife to prevent the cube from "hanging up" in the sabot. The flat and point-launched sabots required no further alterations, however, it was found necessary to remove the corners at the base of the "V" pocket in the edge-launched sabots. Without this modification, the rear corners of the cube would catch on the sabot pocket and the cube would be launched in other than the edge-on configuration.

Sabot separation from the cube was accomplished by a combination of aerodynamic drag and centrifugal forces initiated by the projectile spin.

Appendix C

Solution of the Projectile Spin Equation

The equation for projectile spin stability can be written as

$$\omega^2 \geq \frac{4CDa}{B^2} = \frac{4C\,C_D \rho A V^2 a}{2B^2} \qquad (3)$$

where ω is the minimum rate of spin in rad/sec

C is the transverse moment of inertia

D is the drag force

a is the distance from the mass center to center of pressure (assumed to be on the leading face for flat orientation, on the leading edge for edge orientation, and the leading point for point orientation)

B is the axial moment of inertia

C_D is the drag coefficient

ρ is the density of air

A is the projected surface area

V is the velocity.

The standard cube dimensions and mass were used in all calculations. The moment of inertia about any diagonal through the center of the cube is:

$$C = B = \frac{m\ell^2}{6} \qquad \text{(Ref 22:399, Ref 24:161)}$$

where m is the mass

ℓ is the length of the cube edge

A sample calculation for the launches using the maximum value of $C_D A$ obtained by Hansche and Rhinehart (Ref 9:84) and plotted in Fig. 2 is presented below. Note that the twist required is independent of velocity.

Twist will be defined as length per revolution, thus

$$\text{TWIST}\left(\frac{\text{ft}}{\text{rev}}\right) = \frac{\text{ft/sec}}{\text{rev/sec}\,[0.1592\ \text{rad/rev}]}$$

$$= 6.28\frac{V}{\omega}$$

$$\omega^2 = \frac{39.45\,V^2}{\text{TWIST}^2} \geq \frac{2C_D A\rho V^2 C_a}{B^2}$$

$$C = B = \frac{m\ell^2}{6} = 1.023\ \text{slug}-\text{ft}^2$$

$$\rho_{STD} = 2.3769 \times 10^{-3}\ \text{slug/ft}^3$$

$$\text{TWIST} \leq \frac{0.2878 \times 10^{-2}}{\sqrt{C_D A a}}\ \text{ft}^{\frac{5}{2}} \qquad (14)$$

From Fig. 2, $C_D A = 8.25 \times 10^{-4}\ \text{ft}^2$ and the distances from the center of aerodynamic pressure to mass center are

$^{a}\text{FLAT} = 0.0104$ ft. and TWIST = one turn in 37.3 in.

$^{a}\text{EDGE} = 0.0147$ ft. = one turn in 31.3 in.

$^{a}\text{POINT} = 0.0180$ ft. = one turn in 28.3 in.

Appendix D

Experimental Data

This appendix contains experimental data from the impact orientiation studies, the drag studies, and the ballistic limit testing. Shot number prefixes indicate the cube launch orientation: "F" - Flat, "E" - Edge, and "P" - Point. Shot number suffixes indicate long (L) or short (S) range firings.

Impact Orientation Study

Tables III-V tabulate impact orientation angles and presented impact area for each shot. The error angle concept described on page 12, Section II, was used to determine predominant impact orientation. Shot numbers F-71S, E-26L, and E-40L did not have yaw cards in place. The computer program was run on the IBM 7094 computer. The Fortran statements for this program are on pages 54 and 55.

Drag Study

Tables VI-VIII tabulate the drag coefficient, C_D, as a function of Mach Number. Only shots with identical launch-impact orientation were tabulated.

Ballistic Limit Study

Tables IX-XX tabulate the results of the ballistic limit testing against the four armor materials mentioned on page 16, Section III. Complete or partial penetrations are evaluated under the protection

criteria on page 18, Section III. Note: * indicates shots used for ballistic limits.

```
$IDJOB
$IBFTC CUBES
      DATA FL,ED,PT/5HFLAT ,5HEDGE ,5HPOINT/
  109 FORMAT (23X,4HSHOT,09X,8HRAW DATA,11X,14HADJUSTED ANGLE,10X,11HERR
     1OR ANGLE,7X,9HPRESENTED,2X,4HCUBE,/,22X,6HNUMBER,2X,19HTHETA  PHI
     2   EPSLN,4X,19HTHETA  PHI    EPSLN,4X,17HFLAT  EDGE  POINT,4X,4HAR
     3EA,4X,6HIMPACT,///)
  110 FORMAT (A6,4X,3F10.0)
  112 FORMAT (22X,A6,2X,F4.1,3X,F4.1,3X,F4.1,5X,F4.1,3X,F4.1,3X,F4.1,
     15X,F4.1,2X,F4.1,2X,F4.1,2X,F4.1,3X,1PE8.2,3X,A5)
      WRITE (6,109)
  121 READ (5,110) NAME,A,B,C
      R=57.29578
      X=SIN(A/R)
      Y=SIN(B/R)
      Z=SIN(C/R)
      ERR=1./(X**2+Y**2+Z**2)
      F=SQRT((X**2)*ERR)
      G=SQRT((Y**2)*ERR)
      H=SQRT((Z**2)*ERR)
      DOTF=H
      DOTE=(G+H)/SQRT(2.)
      DOTP=(F+G+H)/SQRT(3.)
      FLAT=ACOS(DOTF)*R
```

```
      EDGE=ACOS(DOTE)*R
      POINT=ACOS(DOTP)*R
      ADJA=ASIN(F)*R
      ADJB=ASIN(G)*R
      ADJC=ASIN(H)*R
      XPL1=1.-(F**2)
      XPL2=-(F*G)
      XPL3=-(F*H)
      YPL1=-(G*F)
      YPL2=1.-(G**2)
      YPL3=-(G*H)
      ZPL1=-(H*F)
      ZPL2=-(H*G)
      ZPL3=1.-(H**2)
      A1=SQRT(((XPL2*ZPL3)-(XPL3*ZPL2))**2+((XPL3*ZPL1)-(XPL1*ZPL3))
     1**2+((XPL1*ZPL2)-(XPL2*ZPL1))**2)
      A2=SQRT(((XPL2*YPL3)-(XPL3*YPL2))**2+((XPL3*YPL1)-(XPL1*YPL3))
     1**2+((XPL1*YPL2)-(XPL2*YPL1))**2)
      A3=SQRT(((YPL2*ZPL3)-(YPL3*ZPL2))**2+((YPL3*ZPL1)-(YPL1*ZPL3))
     1**2+((YPL1*ZPL2)-(YPL2*ZPL1))**2)
      AREA=(A1+A2+A3)*((.25**2)/144.)
      WRITE(6,112) NAME,A,B,C,ADJA,ADJB,ADJC,FLAT,EDGE,POINT,AREA,SYL
      GO TO 121
      END
```

TABLE III

FLAT-LAUNCHED CUBE IMPACT ORIENTATIONS

SHOT NUMBER	RAW DATA THETA	RAW DATA PHI	RAW DATA EPSLN	ADJUSTED ANGLE THETA	ADJUSTED ANGLE PHI	ADJUSTED ANGLE EPSLN	ERROR ANGLE FLAT	ERROR ANGLE EDGE	ERROR ANGLE POINT	PRESENTED AREA	CUBE IMPACT
F-01L	0.	0.	90.0	0.	0.	90.0	-0.	45.0	54.7	4.34E-04	FLAT
F-02L	0.	0.	90.0	0.	0.	90.0	-0.	45.0	54.7	4.34E-04	FLAT
F-03L	0.	0.	90.0	0.	0.	90.0	-0.	45.0	54.7	4.34E-04	FLAT
F-04L	12.4	14.2	75.2	12.1	13.9	71.4	18.6	32.9	36.2	6.07E-04	FLAT
F-05L	0.	0.	90.0	0.	0.	90.0	-0.	45.0	54.7	4.34E-04	FLAT
F-06L	10.1	44.7	47.4	9.8	42.9	45.4	44.6	9.9	25.5	6.78E-04	EDGE
F-07L	0.	0.	90.0	0.	0.	90.0	-0.	45.0	54.7	4.34E-04	FLAT
F-08L	0.	15.6	74.4	0.	15.6	74.4	15.6	29.4	44.7	5.35E-04	FLAT
F-09L	0.	19.6	70.4	0.	19.6	70.4	19.6	25.4	42.5	5.54E-04	FLAT
F-10L	0.	0.	90.0	0.	0.	90.0	-0.	45.0	54.7	4.34E-04	FLAT
F-11L	0.	0.	90.0	0.	0.	90.0	-0.	45.0	54.7	4.34E-04	FLAT
F-12L	0.	22.4	67.6	0.	22.4	67.6	22.4	22.6	41.1	5.67E-04	FLAT
F-13L	0.	0.	90.0	0.	0.	90.0	-0.	45.0	54.7	4.34E-04	FLAT
F-14L	0.	0.	90.0	0.	0.	90.0	-0.	45.0	54.7	4.34E-04	FLAT
F-15L	0.	0.	90.0	0.	0.	90.0	-0.	45.0	54.7	4.34E-04	FLAT
F-16L	0.	0.	90.0	0.	0.	90.0	-0.	45.0	54.7	4.34E-04	FLAT
F-17L	0.	12.4	77.6	0.	12.4	77.6	12.4	32.6	46.5	5.17E-04	FLAT
F-18L	15.2	23.7	65.6	14.8	23.0	62.2	27.8	25.6	28.0	6.64E-04	EDGE
F-19L	0.	0.	90.0	0.	0.	90.0	-0.	45.0	54.7	4.34E-04	FLAT
F-20L	0.	0.	90.0	0.	0.	90.0	-0.	45.0	54.7	4.34E-04	FLAT
F-21L	0.	0.	90.0	0.	0.	90.0	-0.	45.0	54.7	4.34E-04	FLAT
F-22L	0.	0.	90.0	0.	0.	90.0	-0.	45.0	54.7	4.34E-04	FLAT
F-23L	0.	0.	90.0	0.	0.	90.0	-0.	45.0	54.7	4.34E-04	FLAT
F-24L	5.1	14.0	74.7	5..	14.0	75.0	15.0	31.3	41.5	5.63E-04	FLAT

TABLE III (CONTINUED)

FLAT-LAUNCHED CUBE IMPACT ORIENTATIONS

SHOT NUMBER	RAW DATA THETA	RAW DATA PHI	RAW DATA EPSLN	ADJUSTED ANGLE THETA	ADJUSTED ANGLE PHI	ADJUSTED ANGLE EPSLN	ERROR ANGLE FLAT	ERROR ANGLE EDGE	ERROR ANGLE POINT	PRESENTED AREA	CUBE IMPACT
F-25L	0.	0.	90.0	0.	0.	90.0	-0.	45.0	54.7	4.34E-04	FLAT
F-26L	14.3	17.2	71.7	13.9	16.8	67.9	22.1	30.8	32.8	6.32E-04	FLAT
F-27L	0.	0.	90.0	0.	0.	90.0	-0.	45.0	54.7	4.34E-04	FLAT
F-28L	0.	15.4	74.6	0.	15.4	74.6	15.4	29.6	44.8	5.34E-04	FLAT
F-29L	0.	0.	90.0	0.	0.	90.0	-0.	45.0	54.7	4.34E-04	FLAT
F-30L	0.	0.	90.0	0.	0.	90.0	-0.	45.0	54.7	4.34E-04	FLAT
F-31L	0.	0.	90.0	0.	0.	90.0	-0.	45.0	54.7	4.34E-04	FLAT
F-32L	0.	0.	90.0	0.	0.	90.0	-0.	45.0	54.7	4.34E-04	FLAT
F-33L	0.	0.	90.0	0.	0.	90.0	-0.	45.0	54.7	4.34E-04	FLAT
F-34L	0.	0.	90.0	0.	0.	90.0	-0.	45.0	54.7	4.34E-04	FLAT
F-35L	0.	0.	90.0	0.	0.	90.0	-0.	45.0	54.7	4.34E-04	FLAT
F-36L	0.	20.8	69.2	0.	20.8	69.2	20.8	24.2	41.9	5.60E-04	FLAT
F-37L	0.	0.	90.0	0.	0.	90.0	-0.	45.0	54.7	4.34E-04	FLAT
F-38L	0.	0.	90.0	0.	0.	90.0	-0.	45.0	54.7	4.34E-04	FLAT
F-39L	0.	0.	90.0	0.	0.	90.0	-0.	45.0	54.7	4.34E-04	FLAT
F-40L	15.4	28.3	62.7	14.8	27.1	58.6	31.4	22.3	25.5	6.78E-04	EDGE
F-41L	15.4	18.7	73.4	14.7	17.9	66.5	23.5	30.1	31.4	6.42E-04	FLAT
F-42L	0.	13.9	76.1	0.	13.9	76.1	13.9	31.1	45.6	5.26E-04	FLAT
F-43L	14.5	27.5	64.8	13.8	26.2	59.9	30.1	22.5	26.8	6.71E-04	EDGE
F-44L	0.	0.	90.0	0.	0.	90.0	-0.	45.0	54.7	4.34E-04	FLAT
F-45L	17.4	18.8	69.3	16.8	18.2	64.8	25.2	30.6	29.6	6.54E-04	FLAT
F-46L	0.	8.1	80.9	0.	8.1	81.9	8.1	36.9	49.2	4.91E-04	FLAT
F-47L	0.	29.6	63.1	0.	29.0	61.0	29.0	16.0	38.3	5.90E-04	EDGE
F-48L	0.	14.6	75.4	0.	14.6	75.4	14.6	30.4	45.2	5.29E-04	FLAT

TABLE III (CONTINUED)

FLAT-LAUNCHED CUBE IMPACT ORIENTATIONS

SHOT NUMBER	RAW DATA THETA	RAW DATA PHI	RAW DATA EPSLN	ADJUSTED ANGLE THETA	ADJUSTED ANGLE PHI	ADJUSTED ANGLE EPSLN	ERROR ANGLE FLAT	ERROR ANGLE EDGE	ERROR ANGLE POINT	PRESENTED AREA	CUBE IMPACT
F-49L	0.	0.	90.0	0.	0.	90.0	-0.	45.0	54.7	4.34E-04	FLAT
F-50L	0.	0.	90.0	0.	0.	90.0	-0.	45.0	54.7	4.34E-04	FLAT
F-51L	0.	0.	90.0	0.	0.	90.0	-0.	45.0	54.7	4.34E-04	FLAT
F-52L	0.	0.	90.0	0.	0.	90.0	-0.	45.0	54.7	4.34E-04	FLAT
F-53L	0.	0.	90.0	0.	0.	90.0	-0.	45.0	54.7	4.34E-04	FLAT
F-54S	19.1	19.3	63.4	18.9	19.1	62.5	27.5	30.8	27.3	6.68E-04	POINT
F-55S	15.7	19.4	66.9	15.5	19.1	65.0	25.0	29.3	30.0	6.51E-04	FLAT
F-56S	0.	0.	90.0	0.	0.	90.0	-0.	45.0	54.7	4.34E-04	FLAT
F-57S	0.	0.	90.0	0.	0.	90.0	-0.	45.0	54.7	4.34E-04	FLAT
F-58S	0.	0.	90.0	0.	0.	90.0	-0.	45.0	54.7	4.34E-04	FLAT
F-59S	13.1	22.1	63.3	13.2	22.2	63.8	26.2	25.6	29.8	6.52E-04	EDGE
F-60S	0.	0.	90.0	0.	0.	90.0	-0.	45.0	54.7	4.34E-04	FLAT
F-61S	14.9	14.9	74.2	14.5	14.5	69.3	20.7	33.0	34.0	6.23E-04	FLAT
F-62S	0.	0.	90.0	0.	0.	90.0	-0.	45.0	54.7	4.34E-04	FLAT
F-63S	0.	0.	90.0	0.	0.	90.0	-0.	45.0	54.7	4.34E-04	FLAT
F-64S	13.6	15.6	71.9	13.4	15.4	69.4	20.6	31.9	34.2	6.22E-04	FLAT
F-65S	12.7	18.2	70.9	12.5	17.8	68.0	22.0	29.3	33.2	6.29E-04	FLAT
F-66S	0.	0.	90.0	0.	0.	90.0	-0.	45.0	54.7	4.34E-04	FLAT
F-67S	0.	0.	90.0	0.	0.	90.0	-0.	45.0	54.7	4.34E-04	FLAT
F-68S	8.4	21.9	69.6	8.2	21.5	66.9	23.1	24.6	34.4	6.20E-04	FLAT
F-69S	15.8	35.9	56.1	15.0	33.9	52.1	37.9	17.8	22.1	6.97E-04	EDGE
F-70S	0.	23.9	66.1	0.	23.9	66.1	23.9	21.1	40.4	5.73E-04	EDGE
F-72S	0.	0.	90.0	0.	0.	90.0	-0.	45.0	54.7	4.34E-04	FLAT
F-73S	15.8	17.3	67.6	15.7	17.1	66.4	23.6	31.1	31.2	6.43E-04	FLAT

TABLE III (CONTINUED)

FLAT-LAUNCHED CUBE IMPACT ORIENTATIONS

SHOT NUMBER	RAW DATA THETA	PHI	EPSLN	ADJUSTED ANGLE THETA	PHI	EPSLN	ERROR ANGLE FLAT	EDGE	POINT	PRESENTED AREA	CUBE IMPACT
F-74S	13.7	24.7	67.1	13.2	23.7	62.5	27.5	24.3	28.9	6.58E-04	EDGE
F-75S	0.	0.	90.0	0.	0.	90.0	-0.	45.0	54.7	4.34E-04	FLAT
F-76S	0.	19.6	70.4	0.	19.6	70.4	19.6	25.4	42.5	5.54E-04	FLAT
F-77S	18.3	20.3	65.2	17.9	19.9	62.7	27.3	29.7	27.5	6.67E-04	FLAT
F-78S	0.	0.	90.0	0.	0.	90.0	-0.	45.0	54.7	4.34E-04	FLAT
F-79S	16.2	17.4	61.4	16.7	18.0	65.0	25.0	30.8	29.8	6.52E-04	FLAT
F-80S	0.	0.	90.0	0.	0.	90.0	-0.	45.0	54.7	4.34E-04	FLAT
F-81S	0.	0.	90.0	0.	0.	90.0	-0.	45.0	54.7	4.34E-04	FLAT
F-82S	0.	15.3	74.7	0.	15.3	74.7	15.3	29.7	44.8	5.33E-04	FLAT
F-83S	0.	0.	90.0	0.	0.	90.0	-0.	45.0	54.7	4.34E-04	FLAT
F-84S	0.	15.6	74.4	0.	15.6	74.4	15.6	29.4	44.7	5.35E-04	FLAT
F-85S	0.	16.2	73.8	0.	16.2	73.8	16.2	28.8	44.3	5.38E-04	FLAT
F-86S	0.	0.	90.0	0.	0.	90.0	-0.	45.0	54.7	4.34E-04	FLAT
F-87S	0.	0.	90.0	0.	0.	90.0	-0.	45.0	54.7	4.34E-04	FLAT
F-88S	0.	0.	90.0	0.	0.	90.0	-0.	45.0	54.7	4.34E-04	FLAT
F-89S	0.	17.1	72.9	0.	17.1	72.9	17.1	27.9	43.8	5.42E-04	FLAT
F-90S	17.7	19.3	70.7	16.9	18.4	64.6	25.4	30.4	29.3	6.55E-04	FLAT
F-91S	0.	0.	90.0	0.	0.	90.0	-0.	45.0	54.7	4.34E-04	FLAT
F-92S	0.	0.	90.0	0.	0.	90.0	-0.	45.0	54.7	4.34E-04	FLAT

TABLE IV

EDGE-LAUNCHED CUBE IMPACT ORIENTATIONS

SHOT NUMBER	RAW DATA THETA	RAW DATA PHI	RAW DATA EPSLN	ADJUSTED ANGLE THETA	ADJUSTED ANGLE PHI	ADJUSTED ANGLE EPSLN	ERROR ANGLE FLAT	ERROR ANGLE EDGE	ERROR ANGLE POINT	PRESENTED AREA	CUBE IMPACT
E-01L	18.6	32.2	60.6	17.3	29.9	54.5	35.5	21.9	21.6	6.99E-04	POINT
E-02L	34.8	35.8	40.4	33.2	34.1	38.4	51.6	33.3	3.2	7.51E-04	POINT
E-03L	17.1	43.1	51.7	15.8	39.2	46.5	43.5	16.3	19.8	7.07E-04	EDGE
E-04L	0.	30.1	59.9	0.	30.1	59.9	30.1	14.9	37.9	5.93E-04	EDGE
E-05L	21.5	41.3	46.9	20.4	38.9	44.0	46.0	20.6	15.1	7.26E-04	POINT
E-06L	13.0	30.9	61.6	12.5	29.5	57.5	32.5	19.2	26.4	6.73E-04	EDGE
E-07L	14.8	43.9	47.9	14.1	41.5	45.1	44.9	14.2	21.2	7.01E-04	EDGE
E-08L	15.6	40.7	47.8	15.2	39.6	46.4	43.6	15.7	20.3	7.05E-04	EDGE
E-09L	11.7	40.9	52.1	11.2	38.8	49.0	41.0	12.4	24.6	6.84E-04	EDGE
E-10L	24.7	39.5	45.7	23.6	37.5	43.2	46.8	23.8	12.0	7.35E-04	POINT
E-11L	13.7	33.0	57.1	13.3	32.0	54.7	35.3	17.9	24.5	6.84E-04	EDGE
E-12L	11.4	41.0	52.3	10.9	38.8	49.1	40.9	12.1	24.9	6.82E-04	EDGE
E-13L	12.5	41.1	52.0	11.9	38.8	48.7	41.3	13.0	23.8	6.88E-04	EDGE
E-14L	0.	28.7	61.3	0.	28.7	61.3	28.7	16.3	38.4	5.89E-04	EDGE
E-15L	12.7	16.3	73.4	12.4	15.9	69.6	20.4	31.0	34.5	6.19E-04	FLAT
E-16L	13.0	43.4	50.0	12.3	40.7	46.7	43.3	12.7	23.1	6.91E-04	EDGE
E-17L	19.5	26.3	62.7	18.6	25.0	58.0	32.0	26.0	23.4	6.90E-04	POINT
E-18L	23.0	38.1	47.1	22.2	36.6	45.1	44.9	22.7	13.8	7.30E-04	POINT
E-19L	15.0	16.4	75.3	14.4	15.7	68.4	21.6	31.9	33.2	6.29E-04	FLAT
E-20L	16.3	35.8	55.4	15.5	33.9	51.8	38.2	18.2	21.5	6.99E-04	EDGE
E-21L	15.1	21.0	66.4	14.8	20.6	64.2	25.8	27.7	29.4	6.55E-04	FLAT
E-22L	14.8	36.2	55.9	14.1	34.3	52.1	37.9	16.9	22.8	6.93E-04	EDGE
E-23L	15.0	38.0	52.3	14.5	36.5	49.8	40.2	16.1	21.7	6.98E-04	EDGE
E-24L	0.	25.2	64.8	0.	25.2	64.8	25.2	19.8	39.8	5.78E-04	EDGE

TABLE IV (CONTINUED)

EDGE-LAUNCHED CUBE IMPACT ORIENTATIONS

SHOT NUMBER	RAW DATA THETA	RAW DATA PHI	RAW DATA EPSLN	ADJUSTED ANGLE THETA	ADJUSTED ANGLE PHI	ADJUSTED ANGLE EPSLN	ERROR ANGLE FLAT	ERROR ANGLE EDGE	ERROR ANGLE POINT	PRESENTED AREA	CUBE IMPACT
E-25L	20.5	37.5	49.7	19.7	36.0	47.4	42.6	20.7	16.5	7.21E-04	POINT
E-27L	24.8	36.9	49.9	23.3	34.5	46.2	43.8	24.3	13.3	7.31E-04	POINT
E-28L	0.	28.3	61.7	0.	28.3	61.7	28.3	16.7	38.6	5.88E-04	EDGE
E-29L	15.8	30.6	59.7	15.2	29.3	56.2	33.8	20.9	23.9	6.87E-04	EDGE
E-30L	19.7	38.4	51.3	18.7	36.2	47.8	42.2	19.7	17.6	7.17E-04	POINT
E-31L	28.2	42.9	45.4	25.6	38.5	40.7	49.3	25.7	9.7	7.41E-04	POINT
E-32L	15.8	44.3	47.3	15.0	41.7	44.4	45.6	15.1	20.3	7.05E-04	EDGE
E-33L	17.6	41.2	48.9	16.8	39.1	46.1	43.9	17.2	18.8	7.12E-04	EDGE
E-34L	16.5	44.7	47.1	15.6	41.8	44.0	46.0	15.7	19.7	7.08E-04	EDGE
E-35L	0.	30.5	59.5	0.	30.5	59.5	30.5	14.5	37.8	5.94E-04	EDGE
E-36L	11.2	41.3	51.9	10.7	39.2	48.8	41.2	11.8	25.0	6.81E-04	EDGE
E-37L	0.	23.3	66.7	0.	23.3	66.7	23.3	21.7	40.7	5.70E-04	EDGE
E-38L	13.1	39.7	50.8	12.7	38.3	48.8	41.2	13.8	23.1	6.92E-04	EDGE
E-39L	29.4	34.9	47.5	27.7	32.9	44.4	45.6	28.6	9.7	7.41E-04	POINT
E-41L	31.6	37.7	43.5	29.6	35.3	40.5	49.5	29.8	6.3	7.47E-04	POINT
E-42L	19.5	41.5	45.7	18.9	40.0	44.0	46.0	19.0	16.5	7.21E-04	POINT
E-43L	13.5	45.9	47.3	12.8	43.0	44.2	45.8	12.8	22.5	6.95E-04	EDGE
E-44S	26.6	39.7	40.9	26.1	38.8	40.0	50.0	26.1	9.2	7.42E-04	POINT
E-45S	0.	23.0	67.0	0.	23.0	67.0	23.0	22.0	40.8	5.69E-04	EDGE
E-46S	28.0	39.7	45.2	26.2	36.9	41.8	48.2	26.3	9.4	7.42E-04	POINT
E-47S	20.9	30.4	56.2	20.1	29.2	53.3	36.7	24.2	19.3	7.09E-04	POINT
E-48S	0.	18.8	71.2	0.	18.8	71.2	18.8	26.2	42.9	5.51E-04	FLAT
E-49S	23.3	27.8	53.7	23.0	27.5	52.8	37.2	27.2	17.9	7.16E-04	POINT
E-50S	8.7	25.1	62.5	8.7	25.2	63.1	26.9	21.2	31.9	6.38E-04	EDGE

TABLE IV (CONTINUED)

EDGE-LAUNCHED CUBE IMPACT ORIENTATIONS

SHOT NUMBER	RAW DATA THETA	RAW DATA PHI	RAW DATA EPSLN	ADJUSTED ANGLE THETA	ADJUSTED ANGLE PHI	ADJUSTED ANGLE EPSLN	ERROR ANGLE FLAT	ERROR ANGLE EDGE	ERROR ANGLE POINT	PRESENTED AREA	CUBE IMPACT
E-51S	0.	26.9	63.1	0.	26.9	63.1	26.9	18.1	39.1	5.83E-04	EDGE
E-52S	0.	40.1	49.9	0.	40.1	49.9	40.1	4.9	35.6	6.12E-04	EDGE
E-53S	24.7	34.3	49.0	23.9	33.2	47.1	42.9	25.2	13.4	7.31E-04	POINT
E-54S	11.5	35.4	54.9	11.2	34.5	53.2	36.8	14.8	25.6	6.78E-04	EDGE
E-55S	4.0	24.7	66.5	4.0	24.4	65.2	24.8	20.9	36.6	6.04E-04	EDGE
E-56S	12.5	37.8	53.0	12.1	36.5	50.9	39.1	14.2	24.1	6.86E-04	EDGE
E-57S	29.0	32.3	44.7	28.8	32.0	44.3	45.7	29.7	9.3	7.42E-04	POINT
E-58S	13.9	41.0	50.5	13.3	39.1	47.8	42.2	14.1	22.3	6.95E-04	EDGE
E-59S	20.4	26.1	58.8	19.9	25.5	56.7	33.3	26.5	21.9	6.97E-04	POINT
E-60S	14.7	40.5	49.9	14.2	38.9	47.6	42.4	14.9	21.5	7.00E-04	EDGE
E-61S	15.8	28.4	61.8	15.2	27.3	58.1	31.9	22.4	25.0	6.81E-04	EDGE
E-62S	27.5	29.7	55.7	25.6	27.6	50.7	39.3	29.0	15.5	7.25E-04	POINT
E-63S	17.3	36.9	53.1	16.6	35.1	50.0	40.0	18.4	20.1	7.06E-04	EDGE
E-64S	0.	34.4	55.6	0.	34.4	55.6	34.4	10.6	36.6	6.03E-04	EDGE
E-65S	18.3	40.3	48.4	17.6	38.6	46.1	43.9	18.1	18.0	7.15E-04	POINT
E-66S	31.7	38.2	39.5	30.6	36.9	38.1	51.9	30.6	4.7	7.49E-04	POINT
E-67S	24.5	35.6	46.7	24.0	34.8	45.5	44.5	24.8	12.5	7.34E-04	POINT
E-68S	17.3	28.3	60.9	16.7	27.2	57.4	32.6	23.3	23.7	6.88E-04	EDGE
E-69S	18.1	30.5	65.3	16.6	27.9	56.8	33.2	22.8	23.4	6.90E-04	EDGE
E-70S	27.7	30.5	52.9	26.2	28.8	49.2	40.8	28.8	14.1	7.29E-04	POINT
E-71S	0.	28.1	61.9	0.	28.1	61.9	28.1	16.9	38.6	5.87E-04	EDGE
E-72S	23.5	30.9	51.5	23.1	30.3	50.3	39.7	25.7	15.9	7.23E-04	POINT
E-73S	9.2	43.3	47.8	9.0	42.1	46.5	43.5	9.3	26.3	6.74E-04	EDGE
E-74S	0.	14.1	75.9	0.	14.1	75.9	14.1	30.9	45.5	5.27E-04	FLAT

TABLE IV (CONTINUED)

EDGE-LAUNCHED CUBE IMPACT ORIENTATIONS

SHOT NUMBER	RAW DATA THETA	RAW DATA PHI	RAW DATA EPSLN	ADJUSTED ANGLE THETA	ADJUSTED ANGLE PHI	ADJUSTED ANGLE EPSLN	ERROR ANGLE FLAT	ERROR ANGLE EDGE	ERROR ANGLE POINT	PRESENTED AREA	CUBE IMPACT
E-75S	0.	31.6	58.4	0.	31.6	58.4	31.6	13.4	37.4	5.97E-04	EDGE
E-76S	22.1	23.5	56.8	22.1	23.5	56.8	33.2	29.2	21.5	6.99E-04	POINT
E-77S	0.	14.2	74.9	0.	14.3	75.7	14.3	30.7	45.4	5.28E-04	FLAT
E-78S	16.9	27.3	59.9	16.5	26.7	57.9	32.1	23.6	24.1	6.86E-04	EDGE
E-79S	29.9	35.5	42.2	29.3	34.8	41.3	48.7	29.6	6.9	7.46E-04	POINT
E-80S	0.	30.0	60.0	0.	30.0	60.0	30.0	15.0	37.9	5.93E-04	EDGE
E-81S	20.9	39.0	46.6	20.4	37.9	45.1	44.9	20.8	15.3	7.25E-04	POINT
E-82S	21.2	29.3	54.3	20.9	28.8	53.2	36.8	24.9	18.9	7.11E-04	POINT
E-83S	15.9	34.7	53.8	15.5	33.7	51.9	38.1	18.3	21.6	6.99E-04	EDGE
E-84S	8.9	20.5	66.6	9.0	20.6	67.4	22.6	25.6	34.3	6.21E-04	FLAT
E-85S	9.7	39.2	40.0	10.6	43.6	44.5	45.5	10.6	24.7	6.83E-04	EDGE
E-86S	18.3	25.2	56.3	18.6	25.6	57.5	32.5	25.6	23.0	6.92E-04	POINT
E-87S	5.8	26.0	63.6	5.8	25.9	63.3	26.7	19.8	34.2	6.21E-04	EDGE
E-88S	9.3	21.8	65.9	9.3	21.8	66.1	23.9	24.6	33.3	6.28E-04	FLAT
E-89S	8.4	22.7	65.5	8.4	22.7	65.6	24.4	23.5	33.6	6.26E-04	EDGE
E-90S	16.7	32.1	55.7	16.3	31.3	53.8	36.2	20.3	21.9	6.98E-04	EDGE
E-91S	0.	35.4	54.6	0.	35.4	54.6	35.4	9.6	36.4	6.05E-04	EDGE
E-92S	13.8	30.1	57.8	13.6	29.7	56.7	33.3	19.7	25.2	6.80E-04	EDGE
E-93S	14.0	36.5	52.4	13.7	35.7	51.0	39.0	15.9	22.7	6.93E-04	EDGE
E-94S	11.0	41.2	46.6	11.0	41.2	46.7	43.3	11.4	24.4	6.85E-04	EDGE
E-95S	13.3	40.9	49.8	12.9	39.4	47.7	42.3	13.6	22.7	6.93E-04	EDGE

TABLE V

POINT-LAUNCHED CUBE IMPACT ORIENTATIONS

SHOT NUMBER	RAW DATA THETA	RAW DATA PHI	RAW DATA EPSLN	ADJUSTED ANGLE THETA	ADJUSTED ANGLE PHI	ADJUSTED ANGLE EPSLN	ERROR ANGLE FLAT	ERROR ANGLE EDGE	ERROR ANGLE POINT	PRESENTED AREA	CUBE IMPACT
P-01L	13.4	30.9	59.3	13.0	30.0	56.8	33.2	19.1	25.6	6.78E-04	EDGE
P-02L	33.9	37.4	40.6	32.1	35.3	38.3	51.7	32.1	3.6	7.50E-04	POINT
P-03L	13.4	21.0	71.7	12.9	20.1	65.8	24.2	27.3	31.4	6.42E-04	FLAT
P-04L	35.3	31.1	45.4	33.3	29.4	42.6	47.4	34.4	7.7	7.45E-04	POINT
P-05L	22.6	27.8	59.1	21.5	26.4	54.8	35.2	26.8	19.9	7.07E-04	POINT
P-06L	18.3	40.9	50.6	17.2	38.1	46.8	43.2	17.8	18.5	7.13E-04	EDGE
P-07L	26.6	30.6	49.8	26.0	29.9	48.4	41.6	28.2	13.4	7.31E-04	POINT
P-08L	31.7	32.9	46.6	30.1	31.2	43.9	46.1	31.1	8.6	7.43E-04	POINT
P-09L	31.2	33.5	45.8	29.8	32.0	43.4	46.6	30.6	8.3	7.44E-04	POINT
P-10L	14.0	21.7	70.9	13.4	20.8	64.9	25.1	27.0	30.5	6.48E-04	FLAT
P-11L	15.4	34.4	60.6	14.3	31.8	54.4	35.6	18.6	23.6	6.85E-04	EDGE
P-12L	23.0	30.4	57.1	21.7	28.7	52.7	37.3	25.6	18.2	7.14E-04	POINT
P-13L	15.5	18.0	69.3	15.2	17.6	66.4	23.6	30.5	31.2	6.43E-04	FLAT
P-14L	13.6	45.9	48.0	12.8	42.7	44.5	45.5	12.9	22.5	6.95E-04	EDGE
P-15L	24.8	41.9	47.3	22.9	38.3	43.0	47.0	23.1	12.6	7.34E-04	POINT
P-16L	24.1	31.0	56.8	22.6	28.9	51.9	38.1	26.1	17.2	7.18E-04	POINT
P-17L	6.5	39.9	57.8	6.1	36.9	52.4	37.6	9.9	30.1	6.51E-04	EDGE
P-18L	29.2	37.6	44.7	27.7	35.5	42.0	48.0	27.9	8.4	7.44E-04	POINT
P-19L	21.0	40.1	50.2	19.7	37.2	46.2	43.8	20.3	16.2	7.22E-04	POINT
P-20L	16.1	17.8	75.2	15.3	16.9	66.9	23.1	31.1	31.7	6.40E-04	FLAT
P-21L	18.6	35.1	58.8	17.2	32.2	52.4	37.6	20.4	20.6	7.04E-04	EDGE
P-22L	16.5	44.1	48.7	15.5	40.9	45.0	45.0	15.7	19.9	7.07E-04	EDGE
P-23L	20.3	36.6	52.9	19.2	34.4	49.1	40.9	20.8	17.6	7.16E-04	POINT
P-24L	12.7	19.2	74.1	12.2	18.4	67.6	22.4	28.6	33.0	6.30E-04	FLAT

TABLE V (CONTINUED)

POINT-LAUNCHED CUBE IMPACT ORIENTATIONS

SHOT NUMBER	RAW DATA THETA	RAW DATA PHI	RAW DATA EPSLN	ADJUSTED ANGLE THETA	ADJUSTED ANGLE PHI	ADJUSTED ANGLE EPSLN	ERROR ANGLE FLAT	ERROR ANGLE EDGE	ERROR ANGLE POINT	PRESENTED AREA	CUBE IMPACT
P-25L	18.4	40.9	49.2	17.5	38.6	46.2	43.8	18.0	18.1	7.14E-04	EDGE
P-26L	11.0	11.7	76.4	10.9	11.6	74.0	16.0	34.8	38.8	5.86E-04	FLAT
P-27L	0.	28.5	61.5	0.	28.5	61.5	28.5	16.5	38.5	5.89E-04	EDGE
P-28L	18.3	40.2	55.8	16.7	36.1	49.0	41.0	18.0	19.6	7.08E-04	EDGE
P-29L	25.9	33.1	56.9	23.6	30.0	50.1	39.9	26.3	15.6	7.24E-04	POINT
P-30L	10.1	33.4	63.4	9.5	31.1	57.1	32.9	16.4	28.5	6.60E-04	EDGE
P-31L	14.6	43.7	48.8	13.9	41.0	45.7	44.3	14.1	21.5	6.99E-04	EDGE
P-32S	34.0	39.7	41.7	31.2	36.3	38.1	51.9	31.2	4.2	7.50E-04	POINT
P-33S	16.2	22.0	68.5	15.5	21.1	63.3	26.7	27.6	28.5	6.60E-04	FLAT
P-34S	21.8	27.3	59.9	20.8	26.0	55.7	34.3	26.6	20.8	7.03E-04	POINT
P-35S	19.8	36.4	53.5	18.7	34.2	49.6	40.4	20.5	18.2	7.14E-04	POINT
P-36S	14.4	44.1	47.6	13.8	41.8	45.0	45.0	13.9	21.5	6.99E-04	EDGE
P-37S	11.2	30.2	61.7	10.8	29.2	58.5	31.5	18.6	28.1	6.63E-04	EDGE
P-38S	17.5	37.2	53.1	16.7	35.3	49.8	40.2	18.4	19.9	7.07E-04	EDGE
P-39S	0.	13.0	77.0	0.	13.0	77.0	13.0	32.0	46.2	5.21E-04	FLAT
P-40S	29.2	36.2	45.6	27.8	34.3	43.0	47.0	28.2	8.8	7.43E-04	POINT
P-41S	15.8	38.3	55.2	14.8	35.6	50.5	39.5	16.8	21.7	6.99E-04	EDGE
P-42S	9.3	34.9	59.3	8.9	33.2	55.3	34.7	14.4	28.3	6.62E-04	EDGE
P-43S	0.	36.6	53.4	0.	36.6	53.4	36.6	8.4	36.1	6.07E-04	EDGE
P-44S	0.	40.7	49.3	0.	40.7	49.3	40.7	4.3	35.5	6.12E-04	EDGE
P-45S	22.5	22.7	61.2	21.8	22.0	58.2	31.8	30.1	22.9	6.92E-04	POINT
P-46S	13.9	19.5	66.2	13.9	19.4	65.8	24.2	28.3	31.0	6.44E-04	FLAT
P-47S	0.	38.0	52.0	0.	38.0	52.0	38.0	7.0	35.9	6.09E-04	EDGE
P-48S	8.1	22.4	67.1	8.0	22.2	66.2	23.8	23.8	34.1	6.22E-04	EDGE

TABLE V (CONTINUED)

POINT-LAUNCHED CUBE IMPACT ORIENTATIONS

SHOT NUMBER	RAW DATA THETA	PHI	EPSLN	ADJUSTED ANGLE THETA	PHI	EPSLN	ERROR ANGLE FLAT	EDGE	POINT	PRESENTED AREA	CUBE IMPACT
P-49S	32.9	37.5	38.6	31.9	36.4	37.4	52.6	31.9	3.4	7.50E-04	POINT
P-50S	6.3	23.6	64.6	6.3	23.7	65.3	24.7	22.0	34.8	6.17E-04	EDGE
P-51S	30.0	32.7	45.0	29.3	32.0	43.8	46.2	30.2	8.8	7.43E-04	POINT
P-52S	18.1	42.4	45.5	17.6	40.9	43.9	46.1	17.6	17.8	7.16E-04	EDGE
P-53S	9.9	35.4	52.9	9.9	35.4	52.9	37.1	13.4	26.7	6.72E-04	EDGE
P-54S	27.8	33.2	47.3	27.0	32.2	45.6	44.4	28.1	10.9	7.38E-04	POINT
P-55S	20.8	32.1	53.4	20.2	31.2	51.5	38.5	23.2	18.1	7.15E-04	POINT
P-56S	22.8	29.6	54.3	22.2	28.8	52.3	37.7	25.9	17.7	7.16E-04	POINT
P-57S	27.1	36.5	44.3	26.4	35.5	43.0	47.0	26.8	9.7	7.41E-04	POINT
P-58S	24.7	38.5	44.2	24.1	37.4	42.9	47.1	24.3	11.5	7.37E-04	POINT
P-59S	19.8	29.9	56.1	19.3	29.1	54.0	36.0	23.7	20.2	7.05E-04	POINT
P-60S	17.7	31.4	55.7	17.3	30.6	53.9	36.1	21.4	21.3	7.01E-04	POINT
P-61S	24.7	29.1	52.1	24.3	28.6	50.9	39.1	27.5	15.9	7.23E-04	POINT
P-62S	20.7	20.7	63.4	20.2	20.2	60.8	29.2	30.5	25.5	6.78E-04	POINT
P-63S	6.9	26.8	66.0	6.7	26.1	62.9	27.1	19.9	33.3	6.28E-04	EDGE
P-64S	8.1	24.9	67.0	7.9	24.3	64.3	25.7	21.8	33.1	6.30E-04	EDGE
P-65S	7.3	40.3	50.6	7.2	39.6	49.5	40.5	8.8	28.5	6.61E-04	EDGE
P-66S	30.4	34.5	44.4	29.3	33.3	42.7	47.3	29.9	7.8	7.45E-04	POINT
P-67S	23.0	29.4	55.6	22.1	28.3	52.8	37.2	26.1	18.1	7.15E-04	POINT
P-68S	33.3	37.2	39.1	32.1	35.9	37.7	52.3	32.2	3.3	7.51E-04	POINT
P-69S	32.6	33.3	44.7	31.1	31.8	42.4	47.6	31.8	7.2	7.46E-04	POINT
P-70S	20.3	25.1	62.4	19.4	24.0	58.3	31.7	27.2	23.3	6.90E-04	POINT
P-71S	19.7	17.5	69.9	18.9	16.8	64.3	25.7	32.7	29.1	6.57E-04	FLAT
P-72S	25.2	39.2	50.3	23.2	35.7	45.3	44.7	23.8	13.1	7.32E-04	POINT

TABLE V (CONTINUED)

POINT-LAUNCHED CUBE IMPACT ORIENTATIONS

SHOT NUMBER	RAW DATA THETA	RAW DATA PHI	RAW DATA EPSLN	ADJUSTED ANGLE THETA	ADJUSTED ANGLE PHI	ADJUSTED ANGLE EPSLN	ERROR ANGLE FLAT	ERROR ANGLE EDGE	ERROR ANGLE POINT	PRESENTED AREA	CUBE IMPACT
P-73S	25.6	37.4	45.5	24.8	36.1	43.7	46.3	25.2	11.2	7.37E-04	POINT
P-74S	6.3	10.3	77.3	6.3	10.3	77.9	12.1	35.1	43.0	5.50E-04	FLAT
P-75S	17.0	24.4	66.3	16.2	23.3	61.1	28.9	26.1	26.5	6.73E-04	EDGE
P-76S	20.1	28.1	61.6	19.0	26.5	56.5	33.5	25.2	22.0	6.97E-04	POINT
P-77S	13.1	39.3	51.9	12.6	37.7	49.5	40.5	14.0	23.3	6.90E-04	EDGE
P-78S	15.2	38.7	57.2	14.1	35.4	51.1	38.9	16.3	22.5	6.94E-04	EDGE
P-79S	6.3	40.5	53.6	6.1	38.6	50.7	39.3	8.6	29.7	6.53E-04	EDGE
P-80S	27.5	32.7	51.0	26.0	30.9	47.6	42.4	27.8	12.7	7.33E-04	POINT
P-81S	21.6	27.5	61.1	20.4	25.9	56.0	34.0	26.4	21.2	7.01E-04	POINT
P-82S	10.6	30.6	62.4	10.2	29.4	58.6	31.4	18.2	28.6	6.6CE-04	EDGE
P-83S	18.6	22.1	65.3	18.0	21.3	61.5	28.5	28.5	26.4	6.73E-04	POINT
P-84S	25.8	38.9	42.8	25.2	37.9	41.6	48.4	25.3	10.3	7.40E-04	POINT
P-85S	10.6	18.2	72.4	10.4	17.8	69.2	20.8	28.7	34.9	6.17E-04	FLAT
P-86S	18.9	27.3	63.6	17.8	25.7	57.9	32.1	25.1	23.6	6.89E-04	POINT

Table VI

Mach Number and Drag Coefficients
Flat-launched Cubes

Shot Number	M	C_D	Shot Number	M	C_D
F-56S	0.64	1.50	F-7L	1.30	1.52
F-72S	0.73	1.51	F-13L	1.33	1.67
F-67S	0.73	2.25	F-10L	1.34	1.61
F-87S	0.75	1.36	F-41L	1.34	1.72
F-57S	0.77	1.45	F-17L	1.36	1.64
F-66S	0.77	1.51	F-15L	1.37	1.71
F-73S	0.82	1.41	F-16L	1.38	1.67
F-63S	0.85	1.46	F-14L	1.39	1.71
F-85S	0.85	1.47	F-39L	1.41	1.63
F-89S	0.85	1.53	F-12L	1.41	1.68
F-58S	0.85	1.59	F-11L	1.44	1.54
F165S	0.85	1.59	F-8L	1.44	1.77
F-35L	0.86	1.33	F-19L	1.45	1.64
F-68S	0.86	1.40	F-21L	1.45	1.68
F-62S	0.86	1.52	F-26L	1.45	1.72
F-76S	0.87	1.52	F-4L	1.48	1.70
F-78S	0.88	1.57	F-5L	1.48	1.70
F-81S	0.88	1.61	F-23L	1.49	1.64
F-90S	0.88	1.70	F-38L	1.50	1.66
F-84S	0.89	1.64	F-31L	1.52	1.65
F-82S	0.89	1.65	F-33L	1.52	1.66
F-55S	0.90	1.47	F-27L	1.53	1.60
F-60S	0.90	1.46	F-30L	1.53	1.66
F-75S	0.91	1.63	F-25L	1.54	1.62
F-36L	0.93	1.39	F-9L	1.54	1.73
F-61S	0.93	1.50	F-34L	1.58	1.58
F-86S	0.93	1.50	F-24L	1.59	1.59
F-64S	0.93	1.51	F-32L	1.59	1.63
F-54S	0.93	1.62	F-28L	1.60	1.77
F-80S	0.93	1.63	F-2L	1.61	1.62
F-79S	0.94	1.84	F-22L	1.62	1.63
F-88S	0.95	1.59	F-29L	1.63	1.68
F-37L	0.96	1.48	F-20L	1.85	1.67
F-92S	1.04	1.11	F-42L	1.87	1.75
F-91S	1.09	1.74	F-45L	2.20	1.65

Table VI (cont'd)

Mach Number and Drag Coefficients
Flat-launched Cubes

Shot Number	M	C_D	Shot Number	M	C_D
F-1L	2.20	1.68			
F-44L	2.23	1.68			
F-46L	2.25	1.67			
F-48L	2.60	1.63			
F-49L	2.60	1.63			
F-51L	2.99	1.69			
F-50L	3.04	1.66			
F-52L	3.06	1.64			
F-53L	3.37	1.61			

Table VII

Mach Number and Drag Coefficients
Edge-launched Cubes

Shot Number	M	C_D	Shot Number	M	C_D
E-94S	0.46	0.96	E-24L	1.56	1.37
E-52S	0.50	1.09	E-7L	1.56	1.40
E-78S	0.55	0.93	E-6L	1.57	1.44
E-85S	0.56	0.92	E-28L	1.58	1.35
E-51S	0.56	0.98	E-38L	1.59	1.30
E-80S	0.59	1.04	E-36L	1.60	1.37
E-50S	0.61	1.18	E-4L	1.60	1.41
E-58S	0.64	1.03	E-9L	1.61	1.40
E-69S	0.64	1.03	E-13L	1.62	1.47
E-95S	0.64	1.06	E-43L	1.63	1.28
E-90S	0.64	1.07	E-8L	1.63	1.43
E-87S	0.65	1.09	E-22L	1.64	1.34
E-83S	0.66	1.03	E-14L	1.64	1.35
E-61S	0.66	1.02	E-37L	1.65	1.22
E-71S	0.68	1.05	E-12L	1.65	1.38
E-89S	0.68	1.11	E-20L	1.65	1.38
E-63S	0.70	1.07	E-32L	1.65	1.44
E-45S	0.71	1.25	E-3L	1.66	1.37
E-64S	0.72	1.01	E-35L	1.69	1.31
E-60S	0.72	1.04	E-11L	1.70	1.24
E-55S	0.74	1.07	E-16L	1.70	1.40
E-56S	0.74	1.20	E-34L	1.71	1.40
E-68S	0.76	1.08	E-29L	1.72	1.44
E-92S	0.78	1.09	E-33L	1.80	1.34
E-75S	0.79	1.05			
E-54S	0.79	1.26			
E-93S	0.80	1.16			
E-91S	0.81	1.18			
E-73S	0.91	1.21			
E-23L	1.55	1.40			

Table VIII

Mach Number and Drag Coefficients
Point-launched Cubes

Shot Number	M	C_D	Shot Number	M	C_D
P-60S	0.41	0.88	P-5L	1.73	1.32
P-56S	0.50	0.83	P-15L	1.75	1.05
P-68S	0.51	0.86	P-16L	1.79	1.09
P-57S	0.54	0.88	P-29L	1.79	1.10
P-49S	0.54	0.93	P-2L	1.79	1.17
P-55S	0.61	0.82	P-32S	1.90	1.12
P-70S	0.64	0.81	P-72S	1.94	1.15
P-62S	0.64	0.87	P-73S	1.94	1.17
P-59S	0.64	0.91			
P-61S	0.66	0.80			
P-67S	0.74	0.85			
P-54S	0.75	0.89			
P-58S	0.76	0.95			
P-45S	0.76	0.99			
P-66S	0.77	0.93			
P-69S	0.78	0.95			
P-51S	0.89	1.09			
P-83S	1.49	1.32			
P-81S	1.57	1.26			
P-7L	1.58	1.24			
P-80S	1.61	1.18			
P-86S	1.61	1.23			
P-40S	1.62	1.26			
P-19L	1.65	1.19			
P-9L	1.67	1.23			
P-84S	1.67	1.34			
P-34S	1.67	1.17			
P-27L	1.68	1.13			
P-11L	1.69	1.13			
P-23L	1.69	1.14			
P-76S	1.69	1.22			
P-18L	1.72	1.04			
P-4L	1.72	1.20			
P-35S	1.72	1.27			
P-8L	1.73	1.13			

Table IX

Ballistic Limit Testing
2024-T351 Aluminum Plate (0.250 inch)
Flat Impact

Shot Number	Presented Face Area (ft x 10^{-4})	Cube Mass (grains)	V_1 (ft/sec)	V_2 (ft/sec)	V_{impact} (ft/sec)	Results
F-1L	4.42	30.9	2586	2409	2280	Complete
F-2L	4.26	30.8	1896	1768	1680	Complete
F-3L	4.37	30.8	1479	1385	1316	Partial
F-4L	4.38	30.7	1738	1618	1531*	Partial
F-5L	4.38	31.0	1734	1617	1530*	Complete
F-7L	4.33	30.7	1531	1434	1363	Partial
F-8L	4.28	30.8	1696	1573	1484*	Partial
F-9L	4.36	30.8	1818	1687	1592	Complete
F-10L	4.41	31.0	1582	1475	1397	Partial
F-11L	4.34	30.5	1683	1574	1493*	Complete
F-12L	4.39	30.8	1664	1545	1450*	Partial
F-13L	4.40	30.7	1570	1458	1377	Partial
F-14L	4.45	31.1	1642	1525	1440*	Complete
F-15L	4.40	30.8	1617	1502	1418*	Partial
F-16L	4.40	31.0	1628	1515	1433*	Complete
F-17L	4.40	30.7	1602	1494	1413*	Partial
F-19L	4.41	31.0	1705	1589	1504*	Complete

Table IX (cont'd)

Ballistic Limit Testing
2024-T351 Aluminum Plate (0.250 inch)
Flat Impact

Shot Number	Presented Face Area ($ft \times 10^{-4}$)	Cube Mass (grains)	V_1 (ft/sec)	V_2 (ft/sec)	V_{impact} (ft/sec)	Results
E-15L	NA	30.5	1966	1814	1724	Complete
E-19L	NA	30.9	2036	1877	1782	Complete
P-3L	NA	31.1	2004	1841	1725	Complete
P-10L	NA	30.8	1917	1777	1665	Complete
P-13L	NA	30.8	2143	1972	1860	Complete
P-24L	NA	30.7	2193	2016	1893	Complete
P-26L	NA	30.9	2174	2003	1885	Complete
P-33S	NA	31.0	2176	2098	2045	Complete
P-39S	NA	30.8	2086	2017	1968	Complete

Table X

Ballistic Limit Testing
1030 Hot-Rolled Steel Plate (0.125 inch)
Flat Impact

Shot Number	Presented Face Area ($ft \times 10^{-4}$)	Cube Mass (grains)	V_1 (ft/sec)	V_2 (ft/sec)	V_{impact} (ft/sec)	Results
F-20L	4.42	30.8	2181	2025	1913	Complete
F-21L	4.32	30.7	1710	1591	1504	Partial
F-22L	4.37	31.0	1906	1777	1683*	Complete
F-23L	4.36	31.0	1751	1632	1545	Partial
F-24L	4.41	31.1	1870	1745	1654*	Partial
F-25L	4.36	31.0	1810	1688	1599*	Complete
F-26L	4.39	31.0	1708	1585	1496	Partial
F-27L	4.41	31.1	1795	1675	1587*	Complete
F-28L	4.36	30.7	1891	1751	1650*	Partial
F-29L	4.44	30.8	1933	1795	1695*	Complete
F-30L	4.38	30.7	1803	1677	1585*	Partial
F-31L	4.31	30.5	1786	1663	1573	Partial
F-32L	4.35	30.8	1872	1745	1652*	Complete
F-33L	4.39	30.9	1793	1668	1577*	Partial
F-34L	4.40	30.9	1850	1727	1637*	Partial
P-74S	NA	30.8	2046	1966	1920	Complete
P-85S	NA	30.9	1876	1812	1770	Complete
E-21L	NA	30.8	1993	1841	1731	Complete

Table XI

Ballistic Limit Testing
Ballistic Felt (0.5 inch)
Flat Impact

Shot Number	Presented Face Area (ft x 10^{-4})	Cube Mass (grains)	V_1 (ft/sec)	V_2 (ft/sec)	V_{impact} (ft/sec)	Results
F-54S	4.40	31.0	1067	1036	1016	Complete
F-55S	4.37	31.0	1030	1003	986	Complete
F-56S	4.35	30.7	739	719	706	Partial
F-57S	4.35	31.0	886	863	848*	Partial
F-58S	4.36	30.9	980	952	934*	Partial
F-60S	4.36	31.0	1029	1002	985	Complete
F-61S	4.37	31.0	1072	1043	1031	Complete
F-62S	4.32	30.7	989	962	945*	Complete
F-63S	4.38	30.9	982	956	939*	Partial
F-64S	4.37	31.0	1069	1040	1021	Complete
F-65S	4.35	30.7	975	947	929*	Complete
F-66S	4.35	31.0	886	862	847*	Partial
F-67S	4.36	30.9	842	808	786	Partial
F-68S	4.31	30.7	993	968	950*	Complete
F-72S	4.38	30.9	838	815	800	Partial
F-73S	4.38	30.9	937	913	898*	Complete
E-48S	NA	30.7	760	742	730	Complete

Table XII

Ballistic Limit Testing
Ballistic Nylon (12 layer)
Flat Impact

Shot Number	Presented Face Area (ft x 10^{-4})	Cube Mass (grains)	V_1 (ft/sec)	V_2 (ft/sec)	V_{impact} (ft/sec)	Results
F-75S	4.35	31.0	1049	1019	1000*	Partial
F-76S	4.36	30.9	1001	974	957	Partial
F-78S	4.36	31.0	1015	987	969	Partial
F-79S	4.37	31.0	1082	1047	1025*	Complete
F-80S	4.32	30.7	1076	1045	1025*	Partial
F-81S	4.38	30.9	1014	985	966	Partial
F-82S	4.40	31.0	1028	998	979	Partial
F-84S	4.35	31.0	1025	995	976*	Complete
F-85S	4.36	30.9	979	953	936	Partial
F-86S	4.31	30.7	1075	1046	1027*	Partial
F-87S	4.36	31.0	861	840	827	Partial
F-88S	4.37	31.0	1088	1057	1037*	Partial
F-89S	4.32	30.7	983	956	939	Partial
F-90S	4.38	30.9	1010	979	959*	Complete
F-91S	4.37	31.0	1251	1212	1187	Complete
F-92S	4.35	30.7	1190	1166	1151	Partial

Table XII (cont'd)

Ballistic Limit Testing
Ballistic Nylon (12 layer)
Flat Impact

Shot Number	Presented Face Area (ft x 10^{-4})	Cube Mass (grains)	V_1 (ft/sec)	V_2 (ft/sec)	V_{impact} (ft/sec)	Results
E-74S	NA	30.8	981	951	935*	Complete
E-77S	NA	30.9	908	883	865	Complete
E-84S	NA	30.8	835	811	796	Complete
E-88S	NA	30.8	795	773	759	Partial
P-46S	NA	30.8	899	872	853	Complete
P-71S	NA	30.9	706	684	665	Partial

Table XIII

Ballistic Limit Testing
2024-T351 Aluminum Plate (0.250 inch)
Edge Impact

Shot Number	Presented Face Area ($ft \times 10^{-4}$)	Cube Mass (grains)	V_1 (ft/sec)	V_2 (ft/sec)	V_{impact} (ft/sec)	Results
E-3L	5.98	30.8	1964	1809	1697*	Complete
E-4L	6.16	30.8	1890	1733	1620	Partial
E-6L	6.18	30.8	1866	1707	1593	Complete
E-7L	5.99	30.8	1847	1698	1591	Partial
E-8L	6.24	31.0	1932	1768	1650*	Partial
E-9L	6.14	30.8	1907	1750	1637	Partial
E-11L	6.16	30.9	2007	1860	1753	Complete
E-12L	6.07	30.9	1949	1796	1686*	Complete
E-13L	6.15	30.9	1924	1761	1644	Partial
E-14L	6.15	30.9	1931	1779	1669*	Partial
E-20L	6.20	31.0	1955	1799	1687*	Complete
F-6L	NA	30.9	1609	1484	1395	Partial
F-18L	NA	31.0	1626	1510	1415	Partial
P-1L	NA	30.8	2069	1898	1785	Complete
P-6L	NA	30.8	1990	1831	1715*	Partial
P-11L	NA	31.0	2004	1841	1725*	Complete
P-14L	NA	30.9	2043	1878	1764	Complete
P-17L	NA	30.8	2050	1887	1770	Complete

Table XIII (cont'd)

Ballistic Limit Testing
2024-T351 Aluminum Plate (0.250 inch)
Edge Impact

Shot Number	Presented Face Area ($ft \times 10^{-4}$)	Cube Mass (grains)	V_1 (ft/sec)	V_2 (ft/sec)	V_{impact} (ft/sec)	Results
P-21L	NA	30.8	2004	1843	1728	Complete
P-22L	NA	30.8	1986	1832	1720*	Partial
P-25L	NA	30.9	2076	1906	1790	Complete
P-27L	NA	30.9	1993	1829	1711*	Complete
P-28L	NA	30.8	2006	1848	1735	Complete
P-30L	NA	31.6	2071	1907	1790	Complete
P-31L	NA	31.7	2036	1862	1745	Complete
P-36S	NA	30.8	1866	1792	1750*	Partial
P-37S	NA	30.8	1967	1897	1850	Complete
P-38S	NA	30.8	1976	1907	1855	Complete
P-41S	NA	30.9	1958	1879	1832	Complete
P-42S	NA	30.7	1861	1781	1735	Complete

Table XIV

Ballistic Limit Testing
1030 Hot-Rolled Steel Plate (0.125 inch)
Edge Impact

Shot Number	Presented Face Area ($ft \times 10^{-4}$)	Cube Mass (grains)	V_1 (ft/sec)	V_2 (ft/sec)	V_{impact} (ft/sec)	Results
E-16L	6.04	31.0	2006	1847	1732*	Complete
E-22L	6.13	30.8	1932	1782	1674*	Complete
E-23L	6.11	30.7	1831	1683	1577	Partial
E-24L	6.16	30.8	1834	1689	1583	Partial
E-28L	6.01	30.6	1860	1718	1615	Partial
E-29L	6.15	30.8	2040	1871	1750*	Complete
E-32L	6.02	30.6	1953	1794	1680*	Partial
E-33L	6.06	30.5	2124	1955	1833	Complete
E-34L	5.97	30.5	2018	1853	1734*	Complete
E-35L	6.06	30.8	1994	1840	1729*	Complete
E-36L	6.12	30.6	1895	1740	1629*	Partial
E-37L	6.13	30.8	1944	1802	1699*	Partial
E-38L	6.15	30.8	1877	1731	1625*	Partial
E-43L	6.13	30.7	1929	1781	1674*	Partial
P-75S	NA	30.8	2224	2142	2085	Complete
P-77S	NA	30.9	1918	1845	1800	Complete
P-78S	NA	31.0	1972	1898	1848	Complete
P-79S	NA	30.9	1901	1836	1790	Complete
P-82S	NA	30.9	1929	1861	1815	Complete

Table XV

Ballistic Limit Testing
Ballistic Felt (0.5 inch)
Edge Impact

Shot Number	Presented Face Area ($ft \times 10^{-4}$)	Cube Mass (grains)	V_1 (ft/sec)	V_2 (ft/sec)	V_{impact} (ft/sec)	Results
E-45S	6.07	30.7	821	795	778*	Complete
E-50S	6.15	31.0	703	682	669*	Partial
E-51S	6.12	30.7	640	624	614	Partial
E-52S	6.16	30.9	575	559	549	Partial
E-54S	6.07	30.7	912	883	864	Complete
E-55S	6.07	31.0	853	830	815	Complete
E-56S	6.16	30.9	850	824	807	Complete
E-58S	6.05	31.0	736	717	705*	Partial
E-60S	6.12	30.7	826	804	790*	Partial
E-61S	6.16	30.9	761	741	728*	Complete
E-63S	6.07	30.7	810	788	774*	Partial
E-64S	6.07	31.0	826	805	792*	Complete
E-68S	6.15	31.0	872	848	833	Complete
E-69S	6.12	30.7	739	720	708*	Complete
E-71S	6.01	31.0	786	766	753*	Complete
F-59S	NA	30.7	703	682	663	Partial
F-69S	NA	31.0	927	904	885	Complete
F-70S	NA	31.0	826	804	785*	Partial

Table XVI

Ballistic Limit Testing
Ballistic Nylon (12 layer)
Edge Impact

Shot Number	Presented Face Area ($ft \times 10^{-4}$)	Cube Mass (grains)	V_1 (ft/sec)	V_2 (ft/sec)	V_{impact} (ft/sec)	Results
E-73S	6.09	30.8	1043	1011	991	Complete
E-75S	6.08	30.6	893	869	854	Complete
E-78S	6.08	30.8	634	619	609	Partial
E-80S	6.11	30.8	677	659	647	Partial
E-83S	6.09	30.8	764	744	731*	Complete
E-85S	6.08	30.6	638	623	613	Partial
E-87S	6.11	30.9	744	724	711*	Partial
E-89S	6.09	30.8	779	757	743*	Complete
E-90S	6.11	30.8	734	714	701*	Complete
E-91S	6.12	30.8	930	902	884	Complete
E-92S	6.12	30.9	899	874	858	Complete
E-93S	6.09	30.8	920	893	876	Complete
E-94S	6.12	30.8	529	516	508	Partial
E-95S	6.08	30.6	740	720	707*	Partial
F-74S	NA	30.7	996	967	940	Complete
F-77S	NA	30.7	1229	1186	1160	Complete

Table XVI (cont'd)

Ballistic Limit Testing
Ballistic Nylon (12 layer)
Edge Impact

Shot Number	Presented Face Area ($ft \times 10^{-4}$)	Cube Mass (grains)	V_1 (ft/sec)	V_2 (ft/sec)	V_{impact} (ft/sec)	Results
P-43S	NA	30.9	623	606	590	Partial
P-44S	NA	30.8	680	661	645	Partial
P-47S	NA	30.9	735	715	704*	Partial
P-48S	NA	30.9	682	662	646	Partial
P-50S	NA	30.8	669	651	640	Partial
P-52S	NA	30.8	805	783	765*	Complete
P-53S	NA	30.8	557	542	532	Partial
P-63S	NA	30.9	660	642	625	Partial
P-64S	NA	30.9	742	720	703*	Partial
P-65S	NA	30.8	645	627	612	Partial

Table XVII

Ballistic Limit Testing
2024-T351 Aluminum Plate (0.250 inch)
Point Impact

Shot Number	Presented Face Area (ft x 10^{-4})	Cube Mass (grains)	V_1 (ft/sec)	V_2 (ft/sec)	V_{impact} (ft/sec)	Results
P-2L	7.54	30.7	2118	1937	1807*	Complete
P-4L	7.57	31.0	2033	1856	1729*	Partial
P-5L	7.55	30.8	2066	1868	1728*	Complete
P-7L	7.57	31.0	1882	1714	1594	Partial
P-8L	7.51	30.6	2054	1886	1765*	Partial
P-9L	7.57	31.1	1983	1809	1685	Partial
P-11L	7.54	31.0	2004	1841	1724*	Complete
P-12L	7.52	30.8	2058	1892	1772*	Partial
P-15L	7.53	30.6	2064	1906	1792*	Complete
P-16L	7.59	30.8	2120	1952	1831	Complete
P-18L	7.57	30.8	2027	1871	1758*	Partial
P-19L	7.53	30.8	1955	1786	1665	Partial
P-23L	7.66	31.0	1999	1831	1710	Partial
P-29L	7.63	30.8	2122	1949	1825	Complete
P-32S	7.53	30.8	2190	2114	2065	Complete
P-35S	7.54	30.9	1994	1916	1869	Complete
P-34S	7.58	30.6	1931	1860	1815*	Complete
P-40S	7.53	30.7	1875	1802	1756*	Partial

Table XVII (cont'd)

Ballistic Limit Testing
2024-T351 Aluminum Plate (0.250 inch)
Point Impact

Shot Number	Presented Face Area (ft x 10^{-4})	Cube Mass (grains)	V_1 (ft/sec)	V_2 (ft/sec)	V_{impact} (ft/sec)	Results
E-1L	NA	30.8	1835	1682	1572	Partial
E-2L	NA	31.1	1916	1748	1630	Partial
E-5L	NA	30.7	1852	1699	1580	Partial
E-10L	NA	31.0	1926	1761	1640	Partial
E-18L	NA	31.0	1997	1834	1715	Partial

Table XVIII

Ballistic Limit Testing
1030 Hot-Rolled Steel Plate (0.125 inch)
Point Impact

Shot Number	Presented Face Area (ft x 10^{-4})	Cube Mass (grains)	V_1 (ft/sec)	V_2 (ft/sec)	V_{impact} (ft/sec)	Results
P-72S	7.54	30.9	2248	2167	2115	Complete
P-73S	7.58	30.9	2241	2158	2105	Complete
P-76S	7.48	30.8	1953	1879	1832	Complete
P-80S	7.56	30.8	1862	1793	1749*	Complete
P-81S	7.58	30.9	1823	1751	1705*	Partial
P-83S	7.56	31.0	1727	1656	1615	Complete
P-84S	7.50	30.8	1938	1857	1806	Complete
P-86S	7.57	30.9	1865	1793	1750	Complete
E-17L	NA	31.0	1948	1797	1688*	Complete
E-25L	NA	30.9	1829	1682	1635	Partial
E-27L	NA	30.8	1875	1716	1670*	Partial
E-30L	NA	30.4	2003	1840	1723*	Complete
E-31L	NA	30.6	1984	1829	1780*	Partial
E-39L	NA	30.7	2020	1904	1853	Partial
E-41L	NA	30.4	1796	1650	1605	Partial
E-42L	NA	30.8	1854	1694	1579	Partial

Table XIX

Ballistic Limit Testing
Ballistic Felt (0.5 inch)
Point Impact

Shot Number	Presented Face Area (ft x 10^{-4})	Cube Mass (grains)	V_1 (ft/sec)	V_2 (ft/sec)	V_{impact} (ft/sec)	Results
E-44S	NA	31.0	1049	1016	990	Complete
E-46S	NA	31.0	836	814	800*	Partial
E-47S	NA	30.9	1139	1100	1070	Complete
E-49S	NA	31.0	838	816	800	Partial
E-53S	NA	31.0	898	874	860	Complete
E-57S	NA	30.7	667	651	640	Partial
E-59S	NA	31.0	677	507	502	Partial
E-62S	NA	31.0	712	695	680	Partial
E-65S	NA	30.9	809	787	773	Partial
E-67S	NA	31.0	680	663	650	Partial
E-70S	NA	30.9	756	735	720*	Complete

Table XX

Ballistic Limit Testing
Ballistic Nylon (12 layer)
Point Impact

Shot Number	Presented Face Area (ft x 10^{-4})	Cube Mass (grains)	V_1 (ft/sec)	V_2 (ft/sec)	V_{impact} (ft/sec)	Results
P-45S	7.49	30.8	876	849	832	Complete
P-49S	7.52	30.8	618	600	588	Partial
P-51S	7.52	30.8	1030	995	973	Complete
P-54S	7.48	30.8	863	839	824	Complete
P-55S	7.54	30.9	700	682	670	Partial
P-56S	7.58	30.9	575	560	550	Partial
P-57S	7.52	30.8	617	600	589	Partial
P-58S	7.52	30.8	873	847	830	Complete
P-59S	7.52	30.8	740	719	702*	Partial
P-60S	7.53	30.8	473	460	449	Partial
P-61S	7.52	30.8	759	740	728*	Partial
P-62S	7.48	30.8	737	717	704*	Partial
P-66S	7.53	30.8	884	858	841	Complete
P-67S	7.54	30.9	746	726	713*	Complete
P-68S	7.58	30.9	590	574	564	Partial
P-69S	7.52	30.8	900	873	856	Complete
P-70S	7.53	30.8	740	721	709*	Partial

Table XX (cont'd)

Ballistic Limit Testing
Ballistic Nylon (12 layer)
Point Impact

Shot Number	Presented Face Area ($ft \times 10^{-4}$)	Cube Mass (grains)	V_1 (ft/sec)	V_2 (ft/sec)	V_{impact} (ft/sec)	Results
E-72S	NA	30.9	1101	1064	1045	Complete
E-76S	NA	30.9	929	904	885	Complete
E-79S	NA	30.8	834	811	795*	Complete
E-81S	NA	30.8	845	821	804	Complete
E-82S	NA	30.9	808	781	770*	Complete
E-86S	NA	30.9	814	794	781*	Complete

Vita

Randall Lee Schamberger was born [redacted] (PII Redacted) [redacted] He graduated from high school in 1956 and attended St. Petersburg (Florida) Junior College and was graduated with an A.A. degree in 1958. He entered the USAF Academy in June 1958 and in 1962 he received a Bachelor of Science degree with an Engineering Science Major. He attended Undergraduate Navigator Training at James Connally AFB, Texas, and received his wings in June 1963. He has served as test support navigator and flight examiner for the Air Force Eastern Test Range, Patrick AFB, Florida: C-123 navigator and flight examiner in the Republic of South Vietnam; and instructor navigator in the A-26A at England AFB, Louisiana, prior to attendance at graduate school.

Permanent Address: [redacted]

(PII Redacted)

This thesis was typed by Mrs. Mary Catherine Maginn.